Nickel Phosphide Electrocatalysts for Hydrogen Evolution Reaction

Cun Hu [1][ID]**, Chao Lv [1], Shuai Liu [2], Yan Shi [1], Jiangfeng Song [1], Zhi Zhang [1], Jinguang Cai [1,***[ID] **and Akira Watanabe [3]**

[1] Institute of Materials, China Academy of Engineering Physics, Jiangyou 621908, China; hucun402@163.com (C.H.); lvchao219@foxmail.com (C.L.); shiyan@caep.cn (Y.S.); songjiangfeng@caep.cn (J.S.); zhangzhi@caep.cn (Z.Z.)

[2] School of Chemistry and Chemical Engineering, Southwest Petroleum University, Chengdu 610500, China; shuailiu@swpu.edu.cn

[3] Institute of Multidisciplinary Research for Advanced Materials, Tohoku University, 2-1-1 Katahira, Aoba-ku, Sendai 980-8577, Japan; watanabe@tagen.tohoku.ac.jp

* Correspondence: caijinguang@foxmail.com

check for updates

Abstract: The production of hydrogen through electrochemical water splitting driven by clean energy becomes a sustainable route for utilization of hydrogen energy, while an efficient hydrogen evolution reaction (HER) electrocatalyst is required to achieve a high energy conversion efficiency. Nickel phosphides have been widely explored for electrocatalytic HER due to their unique electronic properties, efficient electrocatalytic performance, and a superior anti-corrosion feature. However, the HER activities of nickel phosphide electrocatalysts are still low for practical applications in electrolyzers, and further studies are necessary. Therefore, at the current stage, a specific comprehensive review is necessary to focus on the progresses of the nickel phosphide electrocatalysts. This review focuses on the developments of preparation approaches of nickel phosphides for HER, including a mechanism of HER, properties of nickel phosphides, and preparation and electrocatalytic HER performances of nickel phosphides. The progresses of the preparation and HER activities of the nickel phosphide electrocatalysts are mainly discussed by classification of the preparation method. The comparative surveys of their HER activities are made in terms of experimental metrics of overpotential at a certain current density and Tafel slope together with the preparation method. The remaining challenges and perspectives of the future development of nickel phosphide electrocatalysts for HER are also proposed.

Keywords: nickel phosphide; hydrogen evolution reaction; electrocatalysts; phosphidation reaction; nanocatalysts; water splitting

1. Introduction

The rapid energy depletion and increasing environmental stress necessitate the exploration of sustainable clean energy to replace traditional fossil fuels. Hydrogen has been widely recognized as a promising and sustainable energy carrier to address the above two issues due to its high energy density and environmentally-friendly features [1,2]. An ideal sustainable approach for producing hydrogen is to utilize the electricity produced from clean energy, such as solar cells, to drive the water splitting reaction [3–5], while an efficient hydrogen evolution reaction (HER) electrocatalyst is necessary to reach a high-energy utilization efficiency. It is well-known that Pt-based materials are the most active electrocatalysts for HER, but the large-scale applications are considerably hindered by the high cost and scarcity.

In recent years, plenty of HER electrocatalysts based on earth-abundant transition metal compounds, such as sulphides, selenides, phosphides, nitrides, carbides, and borides, have been

developed with remarkable activities [6–8]. In particular, nickel phosphides, which possess unique electronic properties, efficient electrocatalytic activities, and anti-corrosion features, have attracted significant research attention and are recognized as efficient and low-cost HER catalysts, especially in the acidic electrolyte [9,10]. However, the HER activities of nickel phosphide electrocatalysts are still low for practical applications in electrolyzers, and further studies are necessary. Therefore, at the current stage, a specific comprehensive review is necessary to focus on the progresses of the nickel phosphide electrocatalysts, even though some excellent reviews and perspectives on transition-metal based electrocatalysts for HER or oxygen evolution reaction (OER) have been published [6–8,10–21]. This review is focusing on the developments of preparation approaches of nickel phosphides for HER, which is divided into three main parts: mechanism of HER, properties of nickel phosphides, and preparation and electrocatalytic HER performances of nickel phosphides. The first part will briefly explain the mechanism of HER. The second part will introduce the properties of nickel phosphides. The third part mainly focuses on the progresses of the preparation and HER activities of the nickel phosphide electrocatalysts, which is classified by the preparation method. In this part, the comparative surveys of their activities are made in terms of experimental metrics of overpotential at a certain current density and Tafel slope together with the preparation method. Lastly, the remaining challenges and perspectives of the future development of nickel phosphide electrocatalysts for HER are proposed.

2. Mechanism of HER

Water molecules will be split into hydrogen and oxygen under an external electric field following the reaction equation [22]. H_2O (L) + energy $\rightarrow H_2$ (g) + 1/2O_2 (g). Under standard conditions (298 K, 1 atm), the change of Gibbs free energy ΔG^θ for this reaction is +237.1 kJ mol^{-1}, and the corresponding thermodynamic potential of water electrolysis E is 1.23 V against the reversible hydrogen electrode (RHE) [7]. The reaction of water electrolysis can be divided into two half reactions including a hydrogen evolution reaction (HER) at the cathode and an oxygen evolution reaction (OER) at the anode [23–25]. The mechanism of HER is highly dependent on the pH of the electrolyte. In acidic solutions, the water electrolysis reactions at the cathode and anode take place as follows [15].

$$2H^+ + 2e^- \rightarrow H_2 \text{ (Cathode)}$$

$$H_2O \rightarrow 1/2O_2 + 2H^+ + 2e^- \text{ (Anode)}$$
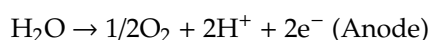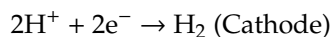
In alkaline solutions, the water electrolysis reactions at the cathode and anode take place as follows [26]

$$2H_2O + 2e^- \rightarrow H_2 + 2OH^- \text{ (Cathode)}$$

$$2OH^- \rightarrow 1/2O_2 + H_2O + 2e^- \text{ (Anode)}$$
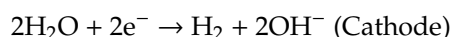
In theory, water electrolysis can be achieved when the overall cell potential is 1.23 V. In fact, the externally applied voltage required to drive water electrolysis is dependent on the thermodynamic potential of water electrolysis and the overpotentials with the reaction on the anode/cathode and ohmic drop of the cells. The externally applied voltage can be defined as follows [27].

$$E_{op} = E_{tp} + \eta_a + \eta_c + iR$$

where E_{op} is the externally applied voltage, E_{tp} is thermodynamic potential of water electrolysis, η_a and η_c are the overpotentials with the reactions on the anode and cathode, respectively, and iR refers to ohmic drop of the cells [28,29]. Therefore, the externally applied voltage must be more than the theoretical voltage of water electrolysis for the reaction to proceed smoothly. High-efficiency catalysts of water electrolysis have high activation energy, which can accelerate the electron transfer and drive the rapid formation of intermediates on the electrode surface. Therefore, it can reduce the overpotentials for water electrolysis.

HER usually occurs on the catalyst surface in one of two different steps and can follow the Volmer–Tafel mechanism or Volmer–Heyrovsky mechanism [11,30,31]. In acidic solutions, the two-electron transfer reaction that occurs on the catalyst surface by two steps is shown in Figure 1 [10]. The first step of HER is called Volmer or the discharge reaction, which discharges protons (H^+) through coupling with an electron on the active surface of the catalyst to form adsorbed hydrogen intermediates (H_{ads}) [32]. The source of protons depends on the pH of the electrolyte. In acidic solutions, it is the hydrogen cation in the electrolyte, while, in alkaline electrolyte, it is the water molecule. In the second step, the formation of the hydrogen molecule in both acidic and basic electrolytes may occur through two different reaction mechanisms, depending on the H_{ads} coverage on the catalyst surface [33]. If the H_{ads} coverage on the surface is large, two adjacent H_{ads} on the electrode surface will recombine with each other to generate a hydrogen molecule, which is called a combination or Volmer-Tafel reaction [34]. If the H_{ads} coverage on the surface is low, the single H_{ads} would prefer to combine with H^+ from the solution and an electron simultaneously to form a hydrogen molecule, which is called the atom + ion or the Volmer-Heyrovsky reaction [35]. For the binding strength of the reaction intermediates, the inherent catalytic activity of the HER catalyst is closely related with the H-adsorption Gibbs free energy (ΔG_{H*}) where * represents the active site on the surface of the catalyst [32]. The ΔG_{H*} can be a good descriptor for determining the HER rate. If the ΔG_{H*} is negative for the catalyst, the H* will bind better to the surface of the electrode and make the Volmer step (initial step) take place very easily. If a catalyst has a large $|\Delta G_{H*}|$ value, the Heyrovsky or Tafel step will be difficult and eventually the entire reaction will become slow. Therefore, the active catalyst for HER needs to have a ΔG_{H*} near zero. It is well-known that the mechanism is distinguished by the Tafel slopes measured during the HER process. If the Volmer reaction (discharge reaction) is fast and the hydrogen molecules are generated by the rate determining combination (Tafel) reaction, the corresponding Tafel slope is 29 mV/dec. If the discharge reaction is fast and the hydrogen molecules are produced by a rate determining atom + ion (Heyrovsky) reaction, the corresponding Tafel slope is 38 mV/dec. If the discharging of H^+ is slow, the hydrogen is evolved either by a rate determining atom + ion reaction or a combination reaction. The corresponding Tafel slope is 116 mV/dec [32].
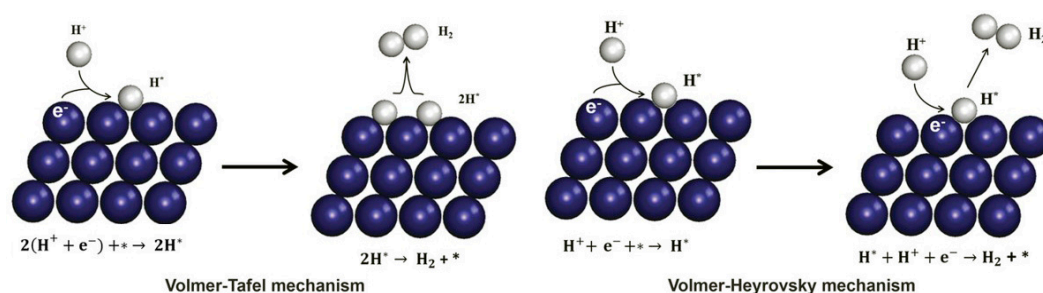

Figure 1. HER mechanisms on the catalyst surface in acidic solutions. Where the * denotes the active sites of the catalyst, H* denotes the adsorbed hydrogen atom at the active site of the catalyst. Reproduced with permission from Reference [33]. Copyright Wiley-VCH, 2019.

3. Properties of Nickel Phosphides

It is well-known that MoS_2 shows high catalytic activities toward both HER and hydrodesulfurization (HDS) [36,37]. Both HDS and HER rely on the catalyst to reversibly combine hydrogen and hydrogen dissociates to produce H_2S in HDS with protons bound to the catalyst to promote the formation of hydrogen in HER [38,39]. These commonalities between the mechanisms and putative active sites of MoS_2 for both HDS and HER catalysis suggest that other materials used for catalytic HDS may also be active electrocatalysts for HER. Typically, Figure 2a shows the crystal structure of the nickel phosphide (Ni_2P), which possesses a hexagonal structure [40], and it has been demonstrated that nickel phosphide (Ni_2P) shows excellent catalytic performance toward HDS [41] and water gas shift reactions for the production of hydrogen [42–44]. Therefore, it can be

speculated that nickel phosphide has electrocatalytic activities toward HER. Nickel phosphides show high physicochemical stability and a superior anticorrosion feature, especially in the acidic electrolyte, which are very important for the applications in the electrolyzers.

As is well-known, in nature, hydrogenase enzymes are a kind of highly efficient biocatalysts to catalyze HER with rapid rates at room temperature. One kind of the hydrogenases has been distinguished as [NiFe] hydrogenases, according to the metal content. Liu et al. studied the behavior of a series of HER catalysts including [NiFe] hydrogenase and the analogues of the $[Ni(PS3^*)(CO)]^{1-}$ and $[Ni(PNP)_2]^{2+}$ complexes as well as surfaces of Ni (111), Pt (111), and Ni_2P (001) through density functional theory (DFT) calculations [39]. They concluded that the catalytic activity of Ni_2P (001) toward HER is associated with an ensemble effect and the presence of P will decrease the number of active Ni sites (Figure 2b,c), which leads to moderate bonding of the intermediates and products with the surface. The P sites also directly participate in the HER. The results suggested Ni_2P as a potential excellent catalyst for HER.

Notably, nickel phosphides have eight mono-phosphides and poly-phosphides with different Ni/P ratios, i.e., Ni_3P, Ni_5P_2, $Ni_{12}P_5$, Ni_2P, Ni_5P_4, NiP, NiP_2, and NiP_3, and the stoichiometric compositions, crystal phases, and crystal facets show influences on the electrocatalytic HER activity. The nickel phosphides of Ni_2P [45], Ni_5P_4 [46], $Ni_{12}P_5$ [47], Ni_3P [48], and NiP_2 [49] phases are generally obtained according to the reported results. Pan et al. investigated the HER performance of different types of nickel phosphides ($Ni_{12}P_5$, Ni_2P, and Ni_5P_4) and found that their catalytic performance followed the order of $Ni_5P_4 > Ni_2P > Ni_{12}P_5$ [50]. It was suggested that the Ni-poor phosphides show a relatively high HER activity. First principle calculations were used to determine the optimal stoichiometry as an HER electrocatalyst among various phases of nickel phosphides. Normally, the hydrogen adsorption free energy (ΔG_H) has been used as a description to correlate the theoretical predictions with the experimental results of the HER activity for various systems. The calculation models for hydrogen adsorbed on the (001) faceted surface of the Ni_4P_5-terminated $Ni_{12}P_5$, Ni_3P_2-terminated Ni_2P, Ni_4P_3-terminated Ni_5P_4, and P-terminated NiP_2 are shown in Figure 2d. It can be seen from the calculation results in Figure 2e that NiP_2 shows the lowest ΔG_H of only -0.16 eV, which suggests the highest HER activity among the four phases. This is consistent with the experimental results [51]. Moreover, some studies have reported the influences of the crystal phase and morphology of nickel phosphides on the catalytic HER performances, which will be discussed in Part 4.1 because the studies are based on the nickel phosphide nanocrystals prepared through the solution phase method. Unfortunately, so far, the dependence of the HER activity on the stoichiometric compositions, crystal phases, and crystal facets for nickel phosphide electrocatalysts has not been fully elucidated yet, which requires further studies.
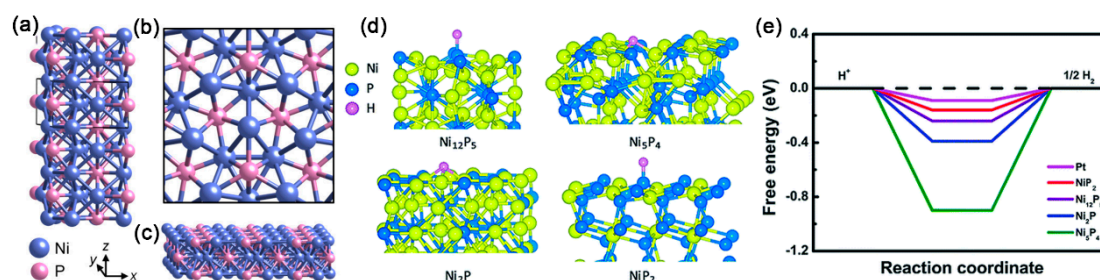

Figure 2. Crystal structure of Ni_2P: four-unit cells stacked on top of one another, with a single unit cell outlined (**a**), top view of the Ni_2P (001) surface (**b**), and a two-dimensional slice of Ni_2P, showing the (001) surface on top (**c**). Reproduced with permission from Reference [45] the American Chemical Society, 2015. Optimized surface structures for the (001) faceted Ni_4P_5-terminated $Ni_{12}P_5$, Ni_3P_2-terminated Ni_2P, Ni_4P_3-terminated Ni_5P_4, and P-terminated NiP_2 (**d**) and corresponding free energy profiles for Pt, Ni$_{12}$P5, Ni_2P, Ni_5P_4, and NiP_2 (**e**). Reproduced with permission from Reference [51]. The Royal Society of Chemistry, 2019.

4. Preparation of Nickel Phosphides and their Electrocatalytic HER Performances

To date, various approaches have been developed to prepare nickel phosphide electrocatalysts, which can be mainly classified into five routes according to the different generation routes of phosphine in nickel phosphides, i.e., solution-phase method, thermal phosphidation with hypophosphite, thermal phosphidation with red phosphorus, hydrogen reduction of phosphates, and electrochemical deposition. In this part, progress on the synthesis of nickel phosphide electrocatalysts and corresponding HER performances are comprehensively reviewed and summarized for a comparison of the preparation approaches.

4.1. Solution-Phase Method

Solution-phase methods, such as the oil-phase reaction, the hydrothermal reaction, and the solvothermal reaction, are generally employed to prepare highly dispersed nanoparticles or nanocrystals. Because of the difficulties in the generation of phosphine species in the environment with oxygen and water, the preparation of nickel phosphide nanostructures is generally carried out in an oil phase solution, which can provide a reduction environment and protect the reaction against oxygen and water. For example, Popczun et al. first proposed a simple solvothermal method to synthesize Ni_2P nanoparticles, which were fulfilled by heating nickel acetylacetonate in 1-octadecene, oleylamine, and trioctylphosphine (TOP) at 320 °C for 2 h [45]. The Ni_2P nanoparticles were obtained through phosphidation of the in-situ formed Ni nanoparticles with TOP. The transmission electron microscope (TEM) image in Figure 3a revealed quasi-spherical nanoparticles with an average diameter of 21 ± 2 nm. The high-resolution TEM (HRTEM) image in Figure 3b clearly showed that the Ni_2P nanoparticles are single crystal and faceted, and the lattice fringes of 5.2 Å correspond to the (100) and (010) planes of Ni_2P. The (001) crystal planes of Ni_2P have been predicted to show higher HER activity. The Ni_2P nanoparticles loaded on a Ti foil electrode exhibit excellent HER performance in 0.5 M H_2SO_4 solution with a low overpotential of 130 mV to achieve a current density of 20 mA/cm^2 (Figure 3c) and a Tafel slope as low as 46 mV/dec (Figure 3d). Moon et al. synthesized Ni_2P nanoparticles through a ligand stabilization method [52], which involves the first preparation of Ni-TOP solution by mixing nickel acetylacetonate and TOP and introducing into the trioctylphosphine oxide (TOPO) under vigorous stirring at 310 °C. The as-prepared Ni_2P electrocatalyst exhibited a high HER activity with a low onset potential for the HER at around −0.02 V vs. RHE and a Tafel slope of 75 mV/dec. Wang et al. reported the preparation of a nanohybrid of carbon nanotubes decorated with $Ni_{12}P_5$ nanocrystals ($Ni_{12}P_5$/CNT) by in situ one-pot hot-solution methods at a relatively mild temperature [47]. The $Ni_{12}P_5$/CNT nanohybrids showed excellent HER performance with a low overpotential of 129 mV for HER at a current density 10 mA/cm^2 and a small Tafel slope of 56 mV/dec. Similarly, Li et al. reported a simple and straight-forward hydrothermal route to grow Ni_2P nanofilms in situ on the surfaces of carbon nanosheets (CNS), which results in strongly coupled 3D structured nanohybrids (Ni_2P/CNS) [53]. The as-prepared Ni_2P/CNS exhibits excellent HER performance in acidic solution and alkaline solution.

Besides nanoparticles and nanocrystals, some other nickel phosphide nanostructures have also been successfully fabricated through the solution phase method for electrocatalytic HER, and the structure-dependent catalytic performance was also studied. For example, Li et al. synthesized nanostructured Ni_2P with different morphologies (nanorods and nanoparticles) by a one-step solution phase route in which the mixture of TOPO and TOP was used as solvent, but their electrocatalytic HER performances were not fully compared [54]. Pan et al. synthesized nickel phosphide (Ni_2P) nanoparticles (NPs) with different sizes through thermal decomposition of bis(triphenylphosphine) nickel dichloride (BTND) single source precursor in the presence of oleylamine by controlling the reaction temperature, and the Ni_2P NPs with a small size exhibit higher electrocatalytic activity due to the larger electrochemical active surface area and higher conductivity [55]. They also reported the synthesis of monodispersed nickel phosphide nanocrystals (NCs) with different phases ($Ni_{12}P_5$, Ni_2P, and Ni_5P_4) via the thermal decomposition approach using nickel acetylacetonate as the nickel

source, TOP as the phosphorus source, and oleylamine in 1-octadecene as the reductant. As shown in Figure 4a, the phases of the nickel phosphide NCs could be easily controlled by changing the P/Ni precursor ratio. The as-synthesized nickel phosphide NCs exhibited good catalytic HER performance, and the HER activity showed a tendency of $Ni_{12}P_5 < Ni_2P < Ni_5P_4$. The superior catalytic activity is attributed to the higher positive charge of Ni and a stronger ensemble effect of P in Ni_5P_4 NCs. Zhang et al. proposed a facile approach for fabricating nanostructured Ni_2P and $Ni_{12}P_5$ by employing phosphonium-based ionic liquid, tetrabutylphosphonium chloride as a novel phosphorus source and reaction medium, upon microwave heating in 1–2 min or conventional heating at 350 °C for 3 h. As shown in Figure 4b, controlling counter anions of various nickel salts could conveniently tune the phase of as-synthesized nickel phosphides. When the $Ni(acac)_2$ and $Ni(OAc)_2 \cdot 4H_2O$ are used as Ni sources, the products are Ni_2P nanoparticles, while the sources of $NiCl_2 \cdot 6H_2O$ and $NiSO_4 \cdot 7H_2O$ produce $Ni_{12}P_5$ nanocrystals. The as-synthesized Ni_2P nanoparticles presented higher catalytic efficiency than $Ni_{12}P_5$. Ni_2P nanoparticles prepared from $Ni(acac)_2$ require an overpotential of only 102 mV to reach 10 mA/cm^2 with a small Tafel slope of 46 mV/dec. This novel ionic liquid-mediated method for the preparation of nickel phosphides shows advantages, that is, it can be operated by microwave heating in a short period of time, which is of particular interest from the viewpoint of energy saving, fast synthesis, and easy operation.
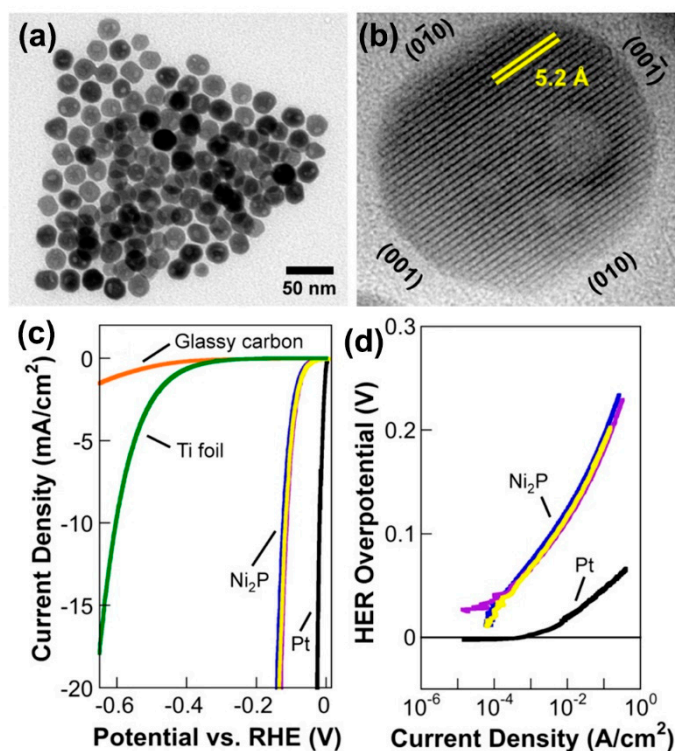
Figure 3. TEM image (**a**) and HRTEM image (**b**) of a representative Ni_2P nanoparticle, highlighting the exposed Ni_2P (001) facet and the 5.2 Å lattice fringes that correspond to the (010) planes. Polarization curves for Ni_2P electrodes, glassy carbon, Ti foil, and Pt in 0.5 M H_2SO_4 for comparison (**c**) and corresponding Tafel plots (**d**). Reproduced with permission from Reference [45], the American Chemical Society, 2015.
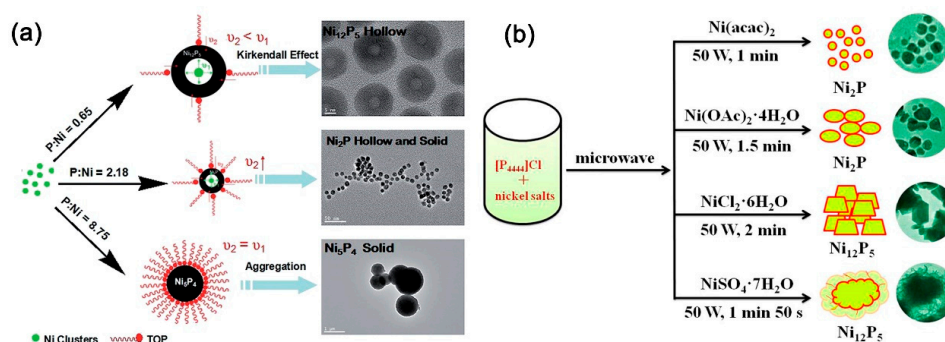
Figure 4. Possible formation mechanism of the as-synthesized nickel phosphide NCs with different phases and morphologies (**a**). Reproduced with permission from Reference [50], Copyright, The Royal Society of Chemistry, 2015. Typical schematic illustration for synthesizing various nickel phosphides controlled by the counter anions of nickel salts (**b**). Reproduced with permission from Reference [56], Copyright, the American Chemical Society, 2018.

Nickel phosphide nanoparticles with different Ni/P ratios can be synthesized by solution-phase reactions, which usually need polymer binders like Nafion to adhere catalysts to the electrodes for HER. Polymer binders generally increase electrical resistance and may reduce active sites, which results in reduced effective catalytic activity and affects long-term stability. Therefore, efforts are devoted to developing approaches for directly growing nickel phosphides on conductive substrates through solution-phase reactions. Wang et al. reported an easy one-step route for the fabrication of an integrated nickel phosphide nanorods/nickel (Ni_2P-NRs/Ni) electrode by direct phosphidation of a commercially available Ni foam current collector under solvothermal conditions using red phosphorus (P) as the precursor [57]. The XRD pattern of the solvothermally-derived product in Figure 5a can be indexed as a hexagonal Ni_2P phase with little admixture of a tetragonal Ni-rich $Ni_{12}P_5$ phase and un-reacted Ni foam underneath. The SEM image in Figure 5b clearly shows the morphology of the nickel phosphides on Ni foam. Densely and vertically arranged NR arrays have formed on the entire surface of the nickel foam ligament. Figure 5c,d are typical dark- and bright-field TEM micrographs, which unambiguously confirm the rod-like shape of the grown Ni_2P. The HRTEM image in Figure 5e shows that the measured inter-planar spacings of 0.28 and 0.25 nm correspond to the distance of (101) and (200) crystal planes of hexagonal Ni_2P, respectively. Corresponding EDX elemental mapping images in Figure 5f further indicate that both Ni and P elements are uniformly distributed on the as-prepared electrode. According to the data in polarization curves (Figure 5g) and Tafel plots (Figure 5h), when used as an integrated cathode in acidic medium, the as-fabricated Ni_2P-NRs/Ni electrode exhibits remarkable electrocatalytic activity toward HER with a small overpotential of 131 mV to attain the current density of 10 mA/cm^2 and a Tafel slope of 106.1 mV/dec. Furthermore, the electrode also shows reasonably good long-term stability. The novel fabrication method reported is scalable and can be extended to obtain other integrated transition metal phosphide/transition metal electrodes, and, therefore, represents an important development toward water electrolyzer cathode materials. Yu et al. fabricated a 3D carbon-coated nickel phosphide nanosheets array on the surface of Ni foam via a simple one-step solvothermal procedure with red phosphorus as the P source [58]. The as-prepared $C@Ni_8P_3$ exhibits excellent HER activity and extraordinary duration in both acidic and basic media. Shi et al. demonstrated the growth of Ni_2P nanosheets on Ni foam by using a low concentration of TOP as a P source [59]. The Ni_2P/Ni, acting as a robust 3D self-supported super-aerophobic hydrogen-evolving cathode, shows superior catalytic performance, stability, and durability in aqueous media over a wide pH value of 0–14. Lai et al. successfully synthesized a rice-shape nanocrystalline Ni_5P_4 on Ni foam by a simple one-step hydrothermal process with sodium hypophosphite as the P source [46]. The Ni_5P_4/NF showed excellent HER performance with a low overpotential of 64 mV at a current density of 10 mA/cm^2 and a small Tafel slope of 64 mV/dec. Some other studies on the preparation of nickel phosphide nanostructures with various morphologies have also been reported through a

one-step hydrothermal method with different phosphorus compounds as the P source (e.g., TOP, sodium hypophosphite, and red phosphorus). All the morphologies, precursors, and corresponding HER performance in acidic or alkaline electrolyte are summarized in Table 1 (acidic) and Table 2 (alkaline) for comparison. Based on the above results, it can be easily found that the solution-phase method generally produces nickel phosphide nanoparticles with different compositions or crystal phases, which can act as model catalysts to study and compare the HER performance between different compositions, crystal phases, or facets and are useful to make catalyst inks for practical applications in membrane electrodes. However, it is difficult to control the morphologies of the nickel phosphides and some of the precursors are high cost for practical use.
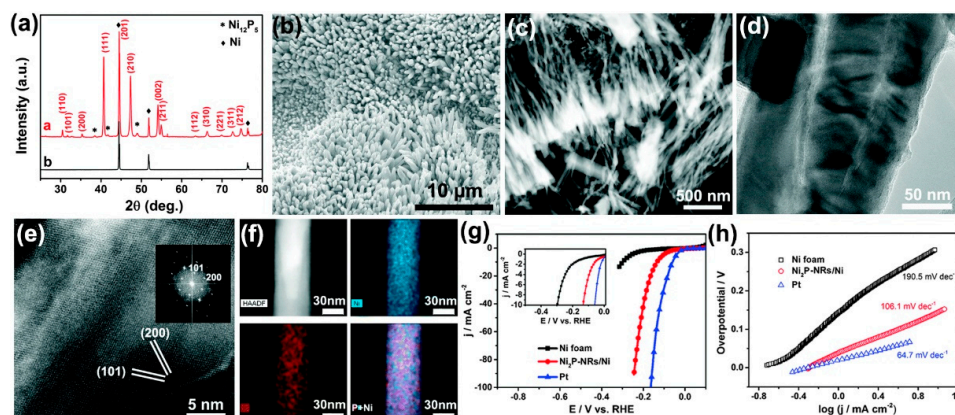

Figure 5. XRD patterns of (**a**) the as-fabricated Ni_2P-NRs/Ni composite electrode, (**b**) SEM image, (**c**) Dark-field, and (**d**) bright-field TEM micrographs of Ni_2P-NRs. (**e**) HRTEM image of a single Ni_2P-NR. Inset: FFT-ED pattern. (**f**) HAADF STEM image of a single NR and the corresponding EDX elemental maps of Ni, P, and Ni + P. (**g**) Polarization curves for Ni_2P-NRs/Ni composite electrode in 0.5 M H_2SO_4. (**h**) The Corresponding Tafel plots. Reproduced with permission from Reference [57]. Copyright the Royal Society of Chemistry, 2015.

Table 1. Summary of the nickel phosphide electrocatalysts prepared through a solution-phase method for HER in an acidic electrolyte.

Material and Morphology	Precursors [1]	Phosphorus Sources [2]	Supports [3]	Loading mg/cm^2	Tafel Slope mV/dec	J mA/cm^2	η mV	Reference
Ni_2P nanocrystals	Ni(acac)$_2$	TPP	Ti foil	~1	70	10	107	[60]
Ni_2P nanosheets	Ni foam	TOP	Ni foam	-	68	1	80	[59]
Ni_8P_3 nanosheet	Ni foam	RP	Ni foam	1.9	46	10	110	[58]
$Ni_{12}P_5$ nanoparticle	Ni(ac)$_2$	TPP	Ti foil	3	63	10	107	[61]
Ni_2P nanoparticles	Ni(acac)$_2$	TOP	GC	0.2	74	10	159	[62]
Ni_2P nanoparticles	NiCl$_2$(Ph$_3$P)$_2$	NiCl$_2$(Ph$_3$P)$_2$	GC	0.199	83.3	20	228	[55]
Ni_2P nanofilms	NiCl$_2$	RP	GC	0.429	64	10	174	[53]
Ni_2P nanorods	Ni foam	RP	Ni foam	-	106.1	10	131	[57]
Ni_5P_4 Nanocrystals	Ni(acac)$_2$	TOP	GC	0.12	51	10	103	[63]
$Ni_{12}P_5$ nanoplates	Ni(acac)$_2$	TOP	Ti foil	1	60.6	10	128	[12]
Ni_2P nanoparticles	Ni(acac)$_2$	TOP	carbon paper	3	55	10	120	[64]
Ni_5P_4 nanoparticles	Ni(acac)$_2$	TOPO	Ti foil	-	33	10	23	[65]
Ni_2P nanoparticles	Ni(acac)$_2$	TOP	GC	0.195	81	10	185	[66]
Ni_2P nanoparticles	Ni(acac)$_2$	TOP	GC	-	74	1	20	[52]
$Ni_{12}P_5$ hollow spheres	NiSO$_4$	NaH$_2$PO$_2$	GC	0.71	46	10	144	[67]
Ni_3P porous hollow nanospheres	NiCl$_2$	NaH$_2$PO$_2$	GC	0.285	50	10	85	[68]
5Ni_5P_4 nanocrystals	Ni(acac)$_2$	TOP	GC	0.199	42	10	34	[50]
Ni_2P nanoparticles	Ni(acac)$_2$	TOP	GC	0.1843	46	10	92	[69]
Ni_2P nanoparticles	Ni(acac)$_2$	TOP	GC	0.1843	59	10	102	[70]
Ni_2P nanoparticles	Ni(acac)$_2$	TOP	Ti foil	1	46	20	130	[45]
Ni_2P nanowires	Ni(acac)$_2$	TOP	GC	0.3	70	20	120	[71]
$Ni_{12}P_5$ nanoparticles	Ni(acac)$_2$	TOP	Ti foils	1.0	56	10	129	[47]
Ni_2P nanowires	Ni(acac)$_2$	TOP	GC	1.42	60	10	133	[72]

[1] Ni(acac)$_2$: nickel acetylacetonate. Ni(ac)$_2$: nickel acetate. NiCl$_2$(Ph$_3$P)$_2$: bis(triphenylphosphine)nickel dichloride.
[2] TPP: triphenylphosphine. TOP: trioctylphosphine. RP: red phosphorous. TOPO: trioctylphosphine oxide. [3] GC: glassy carbon.

Table 2. Summary of the nickel phosphide electrocatalysts prepared through a solution-phase method for HER in alkaline electrolyte.

Material and Morphology	Precursors [1]	Phosphorus Sources [2]	Supports [3]	Loading mg/cm^2	Tafel Slope mV/dec	J mA/cm^2	η mV	Reference
Ni$_2$P Nanosheets	Ni foam	TOP	Ti foil	-	50	1	41	[59]
C@ Ni$_8$P$_3$ nanosheet	Ni foam	RP	Ni foam	1.9	59	10	144	[58]
Ni$_2$P nanofilms	NiCl$_2$	RP	Ni foam	0.429	120	10	315	[53]
Ni$_5$P$_4$ nanoparticles	Ni(acac)$_2$	TOPO	Ti foil	-	98	10	49	[65]
Ni$_2$P/Ni$_{12}$P$_5$ nanoparticles	Ni(NO$_3$)$_2$	RP	GC	-	98	10	234	[73]
Flakelike Ni$_{12}$P$_5$	Ni(ac)$_2$	RP	GC	~3	~106	10	240	[74]
Ni$_2$P nanocrystals	Ni(acac)$_2$	P(Bu)$_4$Cl	GC	0.35	46	10	102	[56]
Multi-shelled Ni$_2$P	NiCl$_2$	NaH$_2$PO$_2$	Ni foam	2	86.4	10	98	[75]
Ni$_5$P$_4$ nanoparticles	NiCl$_2$	NaH$_2$PO$_2$	GC	-	64	10	64	[46]

[1] Ni(acac)$_2$: nickel acetylacetonate. Ni(ac)$_2$: nickel acetate. [2] TOP: trioctylphosphine. RP: red phosphorous. TOPO: trioctylphosphine oxide. P(Bu)$_4$Cl: tetrabutylphosphonium chloride. [3] GC: glassy carbon.

4.2. Thermal Phosphidation with Hypophosphite

Although the solution-phase methods could produce nickel phosphide nanoparticles or nanocrystals with efficient HER activities, it requires effective immobilization of these catalysts on conductive support electrodes using a polymer binder such as Nafion or polytetrafluoroethylene (PTFE) for practical use. These polymer binders generally increase series resistance and may block active sites and inhibit diffusion, which leads to reduced catalytic HER activity. As a result, it is of significant importance to develop a binder-free HER cathode by directly growing the active nickel phosphide catalysts on current collectors. Jiang et al. reported a two-step strategy toward this direction to construct P-rich NiP$_2$ nanosheet arrays supported on carbon cloth (NiP$_2$ NS/CC), which involved the first step to grow Ni(OH)$_2$ nanosheet arrays on CC (Ni(OH)$_2$ NS/CC) hydrothermally followed by converting into NiP$_2$ NS/CC by a low-temperature phosphidation reaction with hypophosphite [76]. The X-ray diffraction (XRD) pattern in Figure 6a clearly indicates the crystal phase of Ni$_2$P. The SEM images of Ni(OH)$_2$ NS/CC in Figure 6b,c and NiP$_2$ NS/CC in Figure 6d,e indicate that the Ni(OH)$_2$ nanosheet precursor on carbon cloth can be converted into NiP$_2$ NS/CC while the structures and morphologies remain unchanged. The corresponding energy dispersive X-ray (EDX) spectrum in Figure 6f shows the atomic ratio between Ni and P to be close to 1:2. The TEM (Figure 6g), HRTEM (Figure 6h), and selected-area electron diffraction (SAED) (Figure 6i) images further confirmed the morphology and crystal phase of the NiP$_2$ nanosheet. The corresponding EDX elemental mapping images in Figure 6j further indicate that both Ni and P elements are uniformly distributed in the whole NiP$_2$ nanosheet arrays. The NiP$_2$ NS/CC electrode exhibits high catalytic performance in acidic solutions with overpotentials of 75 and 204 mV to afford current densities of 10 and 100 mA/cm^2, respectively, a Tafel slope of 51 mV/dec, an exchange current density of 0.26 mA/cm^2, and nearly 100% Faradaic efficiency. Similarly, Cao et al. reported the synthesis of a hollow Ni$_2$P microsphere structure via a facile two-step process, including hydrothermal synthesis of Ni(OH)$_2$ followed by phosphidation with NaH$_2$PO$_2$ under argon [77]. Wang et al. successfully synthesized flower-like nickel phosphide microballs (Ni$_5$P$_4$-MBs) on the surface of a Ti foil substrate by a facile hydrothermal preparation of precursors followed by a post-phosphidation process with hypophosphite (Figure 6k). All possible Ni and P active sites of nickel phosphide were investigated by DFT simulation at a different hydrogen coverage (Figure 6l,m,n). According to the DFT calculation results, the P site of Ni$_5$P$_4$ and NiP$_2$ had an endothermic ΔG_{H^*} of 0.196 and 0.219 eV, respectively, which implies an energetically unfavorable interaction with hydrogen. Therefore, the Ni site of Ni$_5$P$_4$ is the main catalytically active site for the HER. The flower-like Ni$_5$P$_4$ microballs electrocatalyst exhibits excellent activity for the HER with a low overpotential of 35.4 mV to reach a current density of 10 mA/cm^2 and a small Tafel slope of 48 mV/dec in acidic solution. By employing a similar strategy, various structures and morphologies of nickel-containing precursors have been prepared through hydrothermal methods, and then are chemically converted into nickel phosphide electrocatalysts by a low-temperature

phosphidation reaction using hypophosphite as a P source. The structures and morphologies and corresponding electrocatalytic HER performances in acidic or alkaline electrolyte are summarized in Tables 3 and 4, respectively.
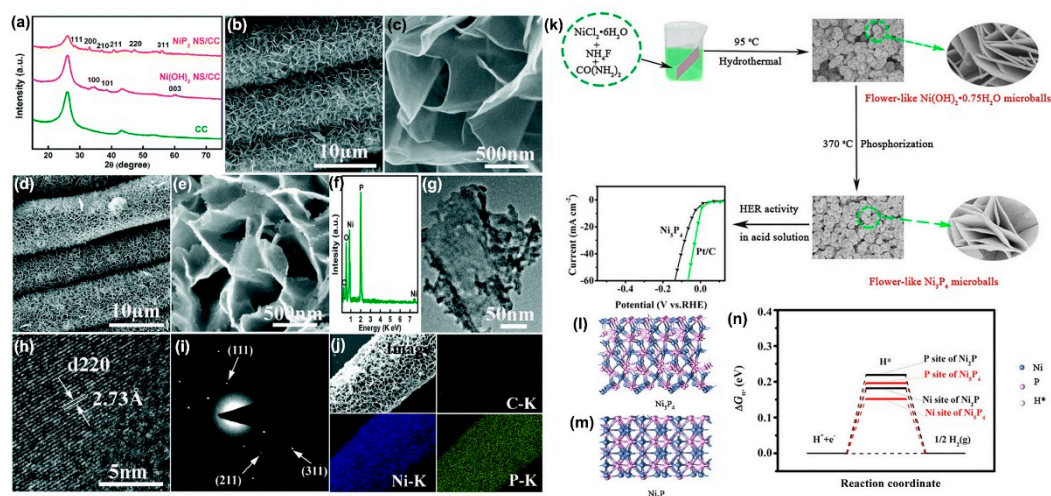

Figure 6. XRD patterns for CC, $Ni(OH)_2$ NS/CC, and NiP_2 NS/CC (**a**), low (**b**) and high (**c**) magnification SEM images of $Ni(OH)_2$ NS/CC, low (**d**) and high (**e**) magnification SEM images and the EDX spectrum (**f**) of NiP_2 NS/CC. TEM (**g**) and HRTEM (**h**) images and SAED pattern (**i**) of NiP_2 NS. STEM image and corresponding EDX elemental mapping images of C, Ni, and P for NiP_2 NS/CC (**j**). Reproduced with permission from Reference [75], Copyright the Royal Society of Chemistry, 2014. Schematic diagram of the growth of Ni_5P_4 and Ni_2P on Ti foil with different morphologies (**k**), DFT-calculated HER activities, top view of the theoretical model of an H atom adsorbed on the Ni sites of a Ni_5P_4 and Ni_2P surface (**l**, **m**) and Gibbs Free energy diagrams for the HER on Ni and P of Ni_5P_4 and Ni_2P, respectively (**n**). Reproduced with permission from Reference [78], Copyright Wiley-VCH, 2018.

Table 3. Summary of the nickel phosphide electrocatalysts prepared through thermal phosphidation with hypophosphite for HER in an acidic electrolyte.

Material and Morphology	Precursors [1]	Supports [2]	Loading mg/cm²	Tafel Slope mV/dec	J mA/cm²	η mV	Reference
$Ni_5P_4/Ni_2P/NiP_2$ Nanocatalysts	$Ni(NO_3)_2$	carbon paper	0.15	46.1	10	62	[79]
Macroporous Ni_2P	$NiCl_2$	Ni foam	2	68.9	20	140	[80]
Ni_2P polyhedrons	$Ni(ac)_2$	GC	0.124	73	10	158	[81]
Ni_2P nanorod	$NiCl_2$	GC	5.34	64	10	186	[82]
Ni_2P Nanosheets	$Ni(NO_3)_2$	Ni foam	-	51	10	75	[83]
Flower-like Ni_5P_4	$NiCl_2$	Ti foil	4.2	48	10	35.4	[78]
Ni_2P nanorod	Ni foam	Ni foam	-	55	10	200	[84]
Ni_5P_4 nanosheet	Ni foam	Ni foam	45	34	10	114	[85]
Ni_5P_4 and Ni_2P nanoparticles	$Ni(NO_3)_2$	GC	0.5	54.5	10	111	[86]
$Ni_{12}P_5/Ni_2P/Ni$ nanowire	Ni foam	Ni foam	31.5	70.8	10	73	[87]
Ni_2P nanoparticles	$Ni(NO_3)_2$	GC	0.35	62	10	172	[88]
Ni_2P nanoparticles	$Ni(NO_3)_2$	GC	0.38	87	20	140	[89]
Ni_2P nanoparticle	$Ni(NO_3)_2$	Ti plate	2	60	10	120	[90]
NiP_2 nanosheet	$Ni(NO_3)_2$	carbon cloth	4.3	51	10	75	[76]
Ni_2P/C microrods	$Ni(NO_3)_2$	GC	0.534	113.2	10	198	[91]
Ni_2P nanoparticles	$Ni(NO_3)_2$	GC	1	56	10	98	[92]
$Ni_2P/graphitic$ carbon hybrid	$Ni(NO_3)_2$	GC	0.633	74	10	166	[93]
Ni_2P nanoarray	$Ni(NO_3)_2$	carbon foil	0.367	67	10	63	[94]
Ni_3P and $Ni_{12}P_5$ nanoparticles	$NiSO_4$	GC	0.6	105	100	333	[95]
Ni_2P nanoparticle	$NiSO_4$	Ti foils	-	84	2	174	[96]
Ni_2P nanoparticle	$Ni(NO_3)_2$	carbon cloth	10.8	55	10	69	[97]
NiP_2 nanosheets	$Ni(NO_3)_2$	carbon cloth	2.8	33.2	10	44	[97]
Ni_2P nanobelts	$NiSO_4$	GC	0.255	62	16	187	[98]

[1] $Ni(ac)_2$: nickel acetate. [2] GC: glassy carbon.

Table 4. Summary of the nickel phosphide electrocatalysts prepared through thermal phosphidation with hypophosphite for HER in an alkaline electrolyte.

Material and Morphology	Precursors [1]	Supports [2]	Loading mg/cm^2	Tafel Slope mV/dec	J mA/cm^2	η mV	Reference
NiP$_2$ Nanorod	NiCl$_2$	carbon paper	0.24	93	10	131	[99]
Ni$_2$P polyhedrons	Ni(NO$_3$)$_2$	GC	0.124	65	10	146	[81]
Urchin-Like Ni$_2$P Superstructures	NiCl$_2$	Ni foam	-	72	10	98	[100]
Nanometric Ni$_5$P$_4$ Clusters	Ni(NO$_3$)$_2$	Ni foam	-	27	10	27	[101]
Ni$_2$P–NiP$_2$ Polymorphs	NiS$_2$	Ni foam	-	58.8	10	59.7	[102]
Ni$_2$P Nanoparticles	NiCl$_2$	melamine foam	-	65	10	92	[103]
Flower-like Ni$_5$P$_4$ microballs	NiCl$_2$	Ti foil	4.2	56	10	47.1	[78]
Ni$_5$P$_4$ nanosheet	Ni foam	Ni foam	45	70	10	190	[85]
Ni$_{12}$P$_5$/Ni$_2$P/Ni nanowire	Ni foam	Ni foam	31.5	115.2	10	148	[87]
Ni2P nanoparticles	NiCl$_2$	GC	0.38	100	20	250	[89]
Ni$_2$P nanosheets	NiCl$_2$	GC	1.63	72.3	10	108	[104]
Ni$_2$P nanoparticles	Ni(NO$_3$)$_2$	GC	1	99	10	188	[92]
Ni$_2$P nanoarray	Ni foam	Ni foam	3.83	76	10	37	[105]
Ni$_2$P nanocrystals	Ni(NO$_3$)$_2$	Ni foam	0.25	58	10	142	[106]
Ni$_{12}$P$_5$/Ni$_2$P nanowire	Ni(ac)$_2$	Ni foam	-	79	10	71	[93]
Ni$_2$P nanoparticle	Ni(NO$_3$)$_2$	carbon cloth	10.8	73	10	73	[97]
Ni$_2$P nanosheet	Ni foam	Ni foam	2.7	90	10	102	[107]
Ni$_2$P-Ni$_5$P$_4$ nanosheet	Ni(NO$_3$)$_2$	carbon cloth	-	83	10	102	[108]
Ni$_2$P nanosheets	Ni foam	Ni foam	3	92	10	134	[109]

[1] Ni(ac)$_2$: nickel acetate. [2] GC: glassy carbon.

Recently, metal–organic frameworks (MOFs) have been proven to be ideal precursors for preparation of a variety of porous nanostructured carbon/metal composites with perfect dispersity of active sites, which can be employed to fabricate nickel phosphide electrocatalysts for the HER. For example, Yan et al. demonstrated the formation of ultrasmall nickel phosphide nanocrystals anchored on reduced graphene oxide (Ni$_2$P/rGO) by implanting Ni-containing MOFs (MOF-74-Ni) on graphene oxide followed by phosphidation with hypophosphite (Figure 7a) [108]. The Ni$_2$P/rGO can be used as highly efficient bifunctional electrocatalysts for overall water splitting. The high magnification SEM image (Figure 7d) and TEM image (Figure 7e) of Ni$_2$P/rGO show that the Ni$_2$P nanocrystals are uniformly anchored on rGO surfaces. The Ni$_2$P/rGO exhibited excellent catalytic performance for both HER and OER in 1.0 M KOH. Furthermore, an electrolyzer employing Ni$_2$P/rGO as a bifunctional catalyst in both the cathode and anode generated 10 mA/cm^2 at a voltage of 1.61 V with excellent stability. Veeramani et al. reported the preparation of a new class of nickel phosphide/graphitic carbon (Ni$_2$P@GC) hybrid through a two-step strategy [93]. They first synthesized Ni-based MOFs (Ni-BTC MOFs) as precursors, and the phosphidation was conducted with sodium hypophosphite to convert Ni-BTC MOFs to Ni$_2$P@GC, which is schematically illustrated in Figure 7b. The SEM image in Figure 6h indicates a stacked layer-like morphology of the precursor Ni-BTC MOF, which was changed to Ni$_2$P nanoparticles on GC after the phosphidation reaction but maintained the overall morphologies (Figure 7i). Similarly, He et al. synthesized nickel phosphide@carbon (Ni$_2$P@C) composites with unique nanorod array morphology via a facile phosphidation process using Ni(II)-zeolitic imidazolate framework-67 (ZIF-67-Ni) as the precursor (Figure 7c) [82]. The Ni$_2$P@C nanorod array exhibited the highest electrocatalytic activity toward HER in 0.5 M H$_2$SO$_4$ solution with a low overpotential of 186 mV at the current density of 10 mA/cm^2 and high durability. By using the same strategy, they also synthesized a hexagonal micro-rod of MOF-74-Ni first via a facile and ultrafast microwave-assisted approach, which was then utilized as a precursor for preparation of a porous Ni$_2$P/C composite. The precursor of the MOF-74-Ni structure (Figure 7f) possesses a hexagonal rod structure with smooth facets and uniform size distribution. Interestingly, the surface of the rod became very rough and numerous pores appeared after the phosphidation reaction with hypophosphite (Figure 7g). The as-prepared Ni$_2$P/C exhibited excellent electrocatalytic activity toward HER with a low onset potential of 94 mV, long-term stability, and a Tafel slope of 113.2 mV/dec. Some other works have also demonstrated the preparation of nickel phosphide electrocatalysts for HER by phosphidation of MOF precursors with

hypophosphite at a relatively low temperature, which are summarized in Tables 3 and 4 based on the acidic or alkaline electrolyte.
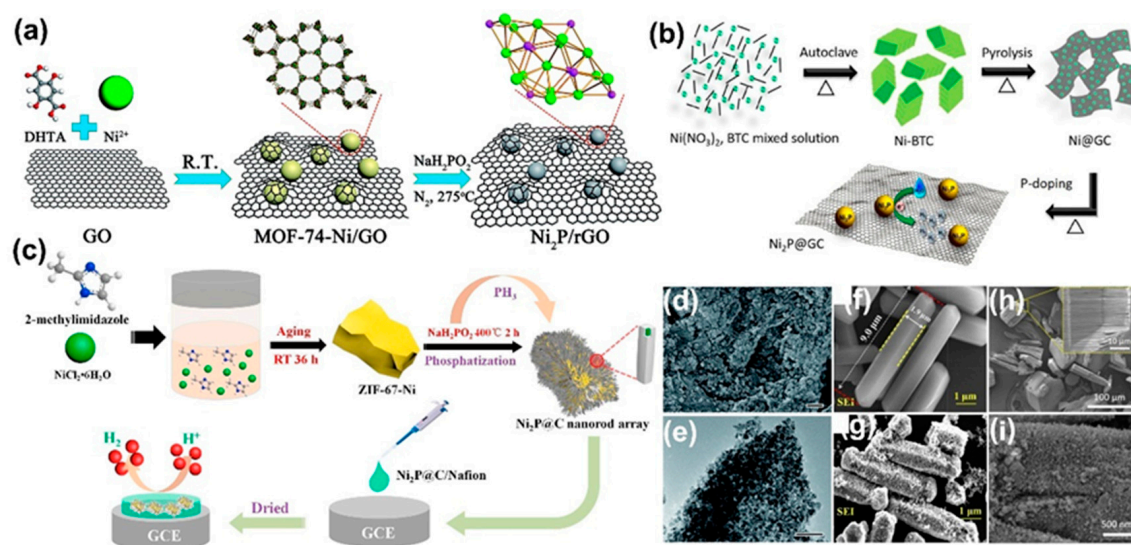

Figure 7. Schematic illustration of the synthesis procedure for the Ni_2P/rGO (**a**), high magnification SEM (**d**), and TEM (**e**) images of the Ni_2P/rGO. Reproduced with permission from Reference [106], Copyright the Royal Society of Chemistry, 2018. Schematic representation for the simple synthesis of Ni@GC and Ni_2P@GC materials (**b**), SEM image of the Ni-BTC precursors (**h**), and SEM image of the Ni@GC samples (**i**). Reproduced with permission from Reference [93], Copyright Elsevier B.V., 2019. Schematic illustration of the preparation process of the Ni_2P@C catalyst and its application as an electrocatalyst for HER (**c**). Reproduced with permission from Reference [82], Copyright Elsevier B.V., 2018. SEM images of MOF-74-Ni (**f**) and Ni_2P/C (**g**). Reproduced with permission from Reference [91], Copyright Elsevier B.V., 2018.

In addition, in spite of that transition, metal nickel has a high abundance and much lower cost as a source for preparation of nickel phosphide electrocatalysts for large-scale hydrogen production through electrochemical water splitting. It may be a more environmentally-friendly and cost-effective way if Ni waste and scrap can be recovered for preparing nickel phosphide electrocatalysts. However, it remains a challenge because of their large amounts of impurities. Recently, Zheng et al. proposed a simple method to synthesize 3D Ni_2P nanoparticles from scrap nickel on carbon cloth (Ni_2P NPs/CC) [110]. As shown in Figure 8a,b, they first dissolved nickel waste in formic acid solution by a simple ultrasonic method. Then NiO nanoparticles were fabricated by photochemical vapor generation and CVD. Lastly, the target product of Ni_2P nanoparticles (NPs) was obtained by phosphidation at a low temperature with hypophosphite. The XRD patterns of NiO NPs (Figure 8c) and Ni_2P NPs/CC (Figure 8d) at different temperatures demonstrated the formation of each crystal phase. It is intriguing that the NiO NPs consist of relatively regular nanoparticles that are 200–300 nm in size (Figure 8e,f). After phosphidation, the surface is composed of relatively loose nanoparticles with a coral-like morphology, as shown in Figure 8g,h. The polarization curves in Figure 8i,k and Tafel plots in Figure 8j,l, respectively, suggested as-prepared Ni_2P NPs possessed significant electrocatalytic performance and excellent stability in both acidic and alkaline media toward the HER with low overpotentials of 69 and 73 mV at 10 mA/cm^2 and small Tafel slopes of 55 and 73 mV/dec, respectively. This strategy is simpler, more cost-effective, and more environmentally-friendly when compared to conventional fabrication methods, which shows potentials in the preparation of multi-functional HER electrocatalysts from more abundant elements for efficient utilization of scrap transition metals.
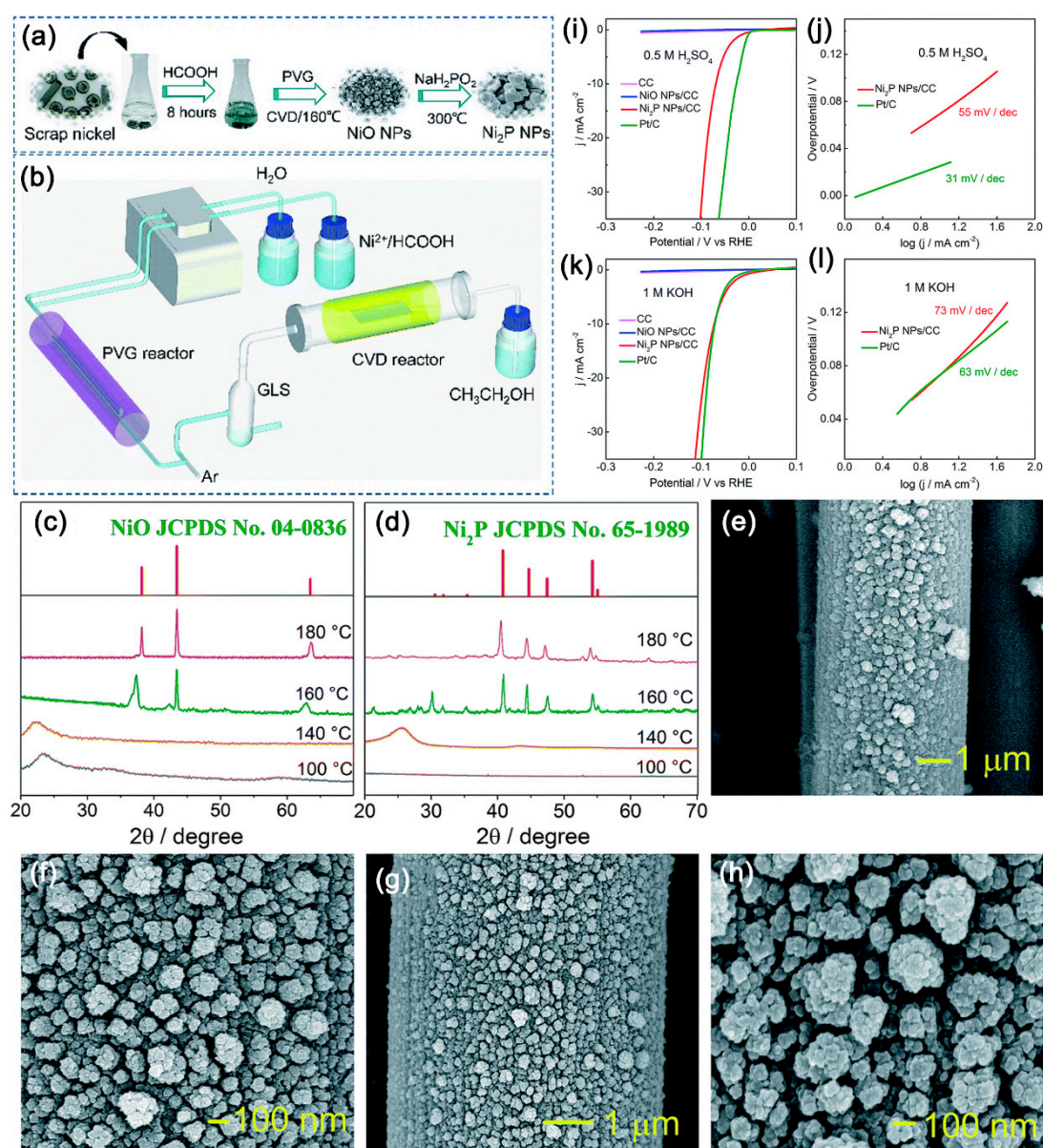
Figure 8. Schematic diagram of Ni$_2$P NPs/CC preparation via acidic extraction, PVG, low-temperature CVD, and phosphidation (**a**) and a detailed diagram of PVG (**b**), XRD patterns of NiO NPs (**c**), and Ni$_2$P NPs/CC (**d**) prepared at 100, 140, 160, and 180 °C, low- (**e**) and high- (**f**) magnification SEM images of NiO NPs/CC prepared at 160 °C. Low- (**g**) and high- (**h**) magnification SEM images of Ni$_2$P NPs/CC. Polarization curves for CC, NiO, and Ni$_2$P NPs/CC obtained at 160 °C in 0.5 M H$_2$SO$_4$ (**i**) and 1 M KOH (**k**), and corresponding Tafel slopes (**j**, **l**). Reproduced with permission from Reference [110], Copyright the Royal Society of Chemistry, 2018.

4.3. Thermal Phosphidation with Red Phosphorus

Although the rational design and growth of nickel compound precursors followed by thermal phosphidation with hypophosphite show potentials to prepare nickel phosphides electrocatalysts with controllable morphologies for efficient HER. The PH$_3$ gases generated during the process (Note: PH$_3$ gases will be released from sodium hypophosphite at ~300 °C [111,112]) are toxic and dangerous to staff. Therefore, gentler phosphidation methods are necessary to lower the risk. A relatively low-toxic red phosphorus powder instead of hypophosphite was employed as a P source in the phosphidation reaction. Ledendecker et al. first demonstrated the simple preparation of highly ordered Ni$_5$P$_4$ nanoarchitectures directly on Ni foil through thermal phosphidation with red phosphorus powder at

550 °C for 1 h under an inert atmosphere [113]. The synthesized Ni_5P_4 nano-architecture electrode exhibits outstanding HER performance in a strong acidic electrolyte. Many interesting morphologies of nickel phosphides prepared by a direct phosphidation reaction method between Ni foam and red phosphorus have been reported because commercial nickel foam holds great promise as a starting material for preparing efficient catalysts due to its unique 3D structure, abundance of macropores, high conductivity, and low price. For example, Wang et al. [114], Mishra et al. [115], and Cai et al. [116] reported the very simple and straight-forward method to fabricate self-supported multi-phase nickel phosphide (e.g., Ni_5P_4-NiP_2 or Ni_5P_4-Ni_2P) nanosheet array cathodes for electrocatalytic HER by placing red phosphorus and commercial nickel foams upstream and downstream of a ceramic crucible, respectively, in the argon atmosphere. In acidic medium, these nickel phosphide nanosheet arrays exhibit very stable and excellent HER performance. Notably, the placement of red phosphorus powder and Ni foam upstream and downstream separately (denoted as F-B method) makes the phosphidation reaction relatively insufficient and low reproducible because the concentration of the P vapor in the reaction tube is significantly influenced by many factors, such as the carry-gas flow rate, the diameter of the tube, and the temperature control. In order to address such issues, we developed a facile, effective, and reproducible phosphidation method by placing a Ni foam above the red phosphorus powder at a distance of 1 cm inside a covered ceramic crucible (denoted as B-U method), which sufficiently allowed the phosphidation reaction [117]. As-prepared self-supported hierarchical porous nickel phosphide (Ni_5P_4/NiP_2) nanosheets exhibited significantly improved HER performance compared to the structures prepared by the general F-B method. Figure 9a,b clearly show the schematic illustration of the B-U method and F-B method, respectively. The SEM images in Figure 9c,d suggest the nickel phosphide (B-U method) nanosheets are uniformly covered on the surface and have relatively small areas with sharp edges and nanopores. XRD patterns of the pristine Ni foam, S_{B-U}, and S_{F-B} are shown in Figure 9e, which indicates that the S_{F-B} shows the Ni_5P_4 phase and unreacted Ni phase, while the S_{B-U} have two nickel phosphide phases, Ni_5P_4 and NiP_2, which suggests the reliability of the B-U method. The polarization curves in Figure 9f and Tafel plots in Figure 9g clearly show that the HER performance of nickel phosphide nanosheets prepared by S_{B-U} method is better than the one prepared by the S_{F-B} method. Alternatively, Laursen et al. prepared Ni_3P microparticles by a conventional solid-state reaction, which allowed Ni (s) and P (s) to react in an evacuated quartz tube at 700 °C for 24 h [48]. The microcrystalline Ni_3P as a noble-metal-free electrocatalyst for HER shows high activity lower than those of Ni_5P_4 and Pt, which are the two most efficient HER catalysts known. Mishra et al. demonstrated the preparation of hierarchical $CoP/Ni_5P_4/CoP$ microsheet arrays via a three-step process [115], i.e., Ni foam was first directly phosphidated at 500 °C in a tube furnace using red phosphorous to form nickel phosphide nanosheet arrays, which was then soaked in Co-ink ($Co(NO_3)_2$ and a DMF mixture solution) followed by a second phosphidation at 500 °C. The as-prepared $CoP/Ni_5P_4/CoP$ microsheet arrays require an ultralow overpotential of only 33 mV at a current density of 10 mA/cm^2. Similarly, Chen et al. prepared Ni_5P_4/NiP_2 nanoparticles on Ni_5P_4/NiP_2 nanosheets by first phosphidation of Ni foam with red phosphorus and dipping in a Ni precursor ink followed by the second phosphidation [118]. As-prepared hierarchical nickel phosphide structures exhibit an overpotential of only 35 mV at a current density of 10 mA/cm^2 in an acidic solution and great stability at a high current density of 1200 mA/cm^2.
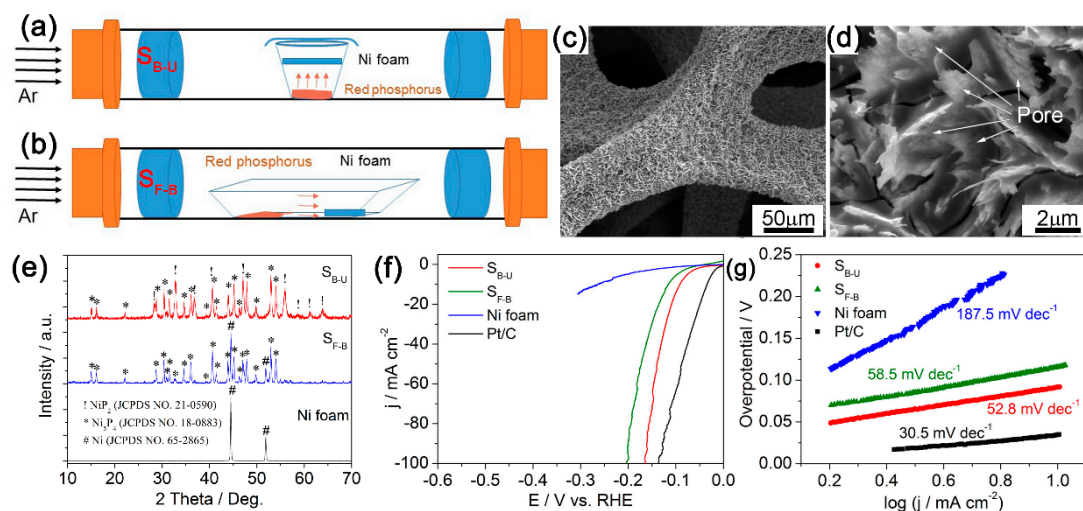
Figure 9. Schematic illustration for preparation of nickel phosphide by the method with bottom-up placement S$_{B-U}$ (**a**) and an upstream-downstream placement S$_{F-U}$ (**b**). Low- (**c**) and high- (**d**) magnification SEM images of S$_{B-U}$. XRD patterns of the S$_{B-U}$ (500 °C), S$_{F-B}$ (500 °C), and the pristine Ni foam (**e**). Polarization curves (**f**) and Tafel plots (**g**) of the S$_{B-U}$ (500 °C), S$_{F-B}$ (500 °C), pristine Ni foam, and Pt/C catalyst. Reproduced with permission from Reference [117], Copyright Elsevier B.V., 2019.

Nickel phosphides discussed above were synthesized by direct phosphidation of Ni foam or Ni foil with red phosphorous. Two issues should be considered in practical use when using metal Ni as precursors, i.e., the dissolution behavior of the unphosphidated Ni during electrocatalytic water splitting and the fragility of the nickel phosphide structures. Therefore, an alternative process should be developed to address such issues. Wang et al. reported a convenient and scalable approach for fabricating a self-supported 3D carbon fiber paper electrode deposited with vertically aligned Ni-P nanosheets (NSs) as bifunctional catalysts for HER and OER through electrodeposition of the Ni layer on the surface of carbon microfibers followed by a simple direct phosphidation process [119]. The self-supported 3D electrode can be directly used as either a cathode to drive HER or an anode to expedite OER, which exhibits excellent electrocatalytic activity and outstanding long-term durability. Recently, our group developed a general, facile, and scalable method to prepare nickel phosphide (Ni$_5$P$_4$/NiP$_2$/Ni$_2$P) porous nanosheets with high electrocatalytic HER activities through electroless Ni plating on arbitrary substrates, which is followed by a simple direct phosphidation reaction [120]. The preparation of the porous nickel phosphide nanosheets on carbon cloth is schematically shown in Figure 10a. The polarization curves in Figure 10b clearly show that the nickel phosphide electrode exhibits excellent HER performance in 0.5 M H$_2$SO$_4$ solution with very low overpotentials of 63 mV and 120 mV to achieve current densities of 10 mA/cm^2 and 100 mA/cm^2, respectively. Furthermore, a time-dependent potential curve in Figure 10c indicates that the electrode exhibits outstanding durability for 168 h under a constant current density of 10 mA/cm^2. The SEM images of Ni/CC-60 and Ni-P/CC-60-450 shown in Figure 10d,e,f,g, respectively, indicate that the carbon fibers are uniformly covered by high-density novel porous nickel phosphide nanosheets. This strategy was demonstrated in the preparation of porous nickel phosphide nanostructures on leaf vein (LV) and silkworm cocoon (SC), which are both highly active electrocatalysts for HER. The SEM images of Ni-P/LV in Figure 10h,i show that the nickel phosphide nanosheets are very thin and have many inner pores. The SEM images of Ni-P/SC in Figure 10j,k indicate that the nickel phosphide nanowires have relatively sharp tips and some pores inside. Therefore, this strategy is a general method to prepare transition-metal compound nanostructures in a facile, stable, and scalable way for various practical applications.
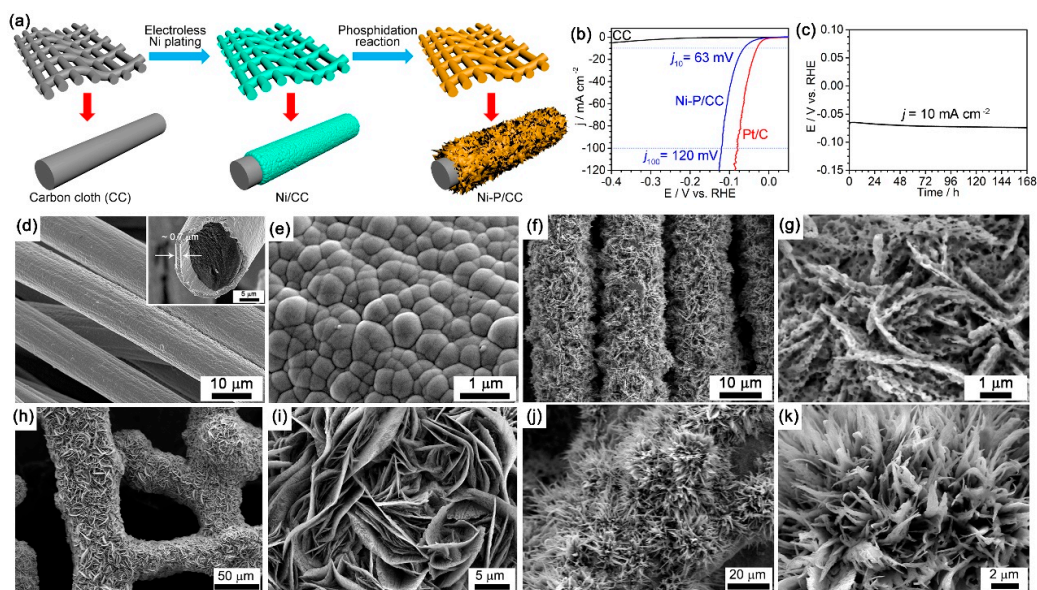
Figure 10. Schematic illustration for preparation of porous nickel phosphide nanosheets on carbon cloth (**a**), polarization curves for the carbon cloth (CC), Pt/CC, and Ni-P/CC electrode in 0.5 M H_2SO_4 (**b**), time-dependent potential curve of the Ni-P/CC-60-450 in 0.5 M H_2SO_4 electrolyte under a constant current density of 10 mA cm^{-2} for 168 h (**c**). Low- (**d**) and high- (**e**) magnification SEM images of the Ni/CC-60. Inset in (**d**) is a typical cross-sectional SEM image of one fiber in the Ni/CC-60. Low- (**f**) and high- (**g**) magnification SEM images of the Ni-P/CC-60-450. SEM images of the Ni-P/LV (**h,i**) and Ni-P/SC (**j,k**). Reproduced with permission from Reference [120], Copyright The American Chemical Society, 2019.

In addition, Ni-containing precursors instead of Ni forms or Ni layer plating can be synthesized by the electrospinning process, the hydrothermal method, or a direct annealing growth method. For instance, Kim et al. successfully prepared nickel phosphide embedded in carbon nanofibers (Ni-P/CNFs) through an electrospinning process followed by a simple direct phosphidation method [51]. Figure 11a shows the schematic illustration for the synthesis of the Ni-P/CNFs. The TEM images of the Ni/CNFs in Figure 11b and Ni-P/CNFs in Figure 11c indicate that the nickel nanoparticles and nickel phosphide nanoparticles are embedded in carbon nanofibers, respectively. The Ni-P/CNFs electrode exhibits excellent HER performance in 0.5 M H_2SO_4 solution with a low overpotential of 71 mV to achieve a current density of 10 mA cm^{-2} with a small Tafel slope of 74 mV/dec and excellent catalytic stability over 100 h (Figure 11d,e). Cao et al. successfully synthesized vertically aligned NiP_2 nanosheets on Ti foil via a facile two-step process [49]. As shown in Figure 11f, the precursor of $Ni(OH)_2$ nanosheets was first prepared on Ti foil through a facile hydrothermal method, and then was transformed into NiP_2 nanosheets by thermal phosphidation with red phosphorus. The SEM images of $Ni(OH)_2$ nanosheets in Figure 11g and NiP_2 nanosheets in Figure 11h indicate that $Ni(OH)_2$ nanosheets were successfully converted into NiP_2 nanosheets with the structures and morphologies maintaining. Yan et al. proposed an effective synthetic method to obtain self-supported, hierarchical, and edge-rich nickel phosphide nanosheet arrays on nickel foam (Ni_2P NSs-NF), which were successfully employed as a high-efficiency, 3D binder-free electrode for HER. The Ni-precursor on Ni foam was prepared via a facile direct annealing growth method, and then the Ni-precursor was converted into hierarchical edge-rich Ni_2P nanosheet arrays via a direct phosphidation reaction at 500 °C with red phosphorus. The Ni_2P NSs-NF electrode exhibits superior activity for the HER both in alkaline and acidic conditions. Generally, the direct phosphidation reaction with red phosphorus is carried out at a relatively high temperature of ~500 °C. In order to solve this issue, Wu et al. successfully realized the temperature lowering down to 250 °C by using H_2 plasma-activated red phosphorus, which enables the synthesis of self-supported Ni_2P nanosheet (Ni_2P/NF) arrays on commercial nickel foam from a NiO/NF precursor [121]. The

obtained electrode exhibits an excellent hydrogen evolution activity in an acidic electrolyte and also good mechanical strength. The morphologies and HER performance in acidic and alkaline electrolytes of the nickel phosphide electrocatalysts prepared by thermal phosphidation with red phosphorus are summarized in Tables 5 and 6, respectively, for comparison. Although the approach of thermal phosphidation with red phosphorus shows relatively high safety compared to that with hypophosphite and potentials in the preparation of nickel phosphide electrocatalysts with high HER performance, the studies using this method are relatively fewer and mainly focus on the Ni metal precursors. Rare works have involved the control on the structures and morphologies. Therefore, studies are still required to exert the full potentials of this method on the production of nickel phosphide electrocatalysts with controllable structures, morphologies, components, crystal phases, and high HER activities.
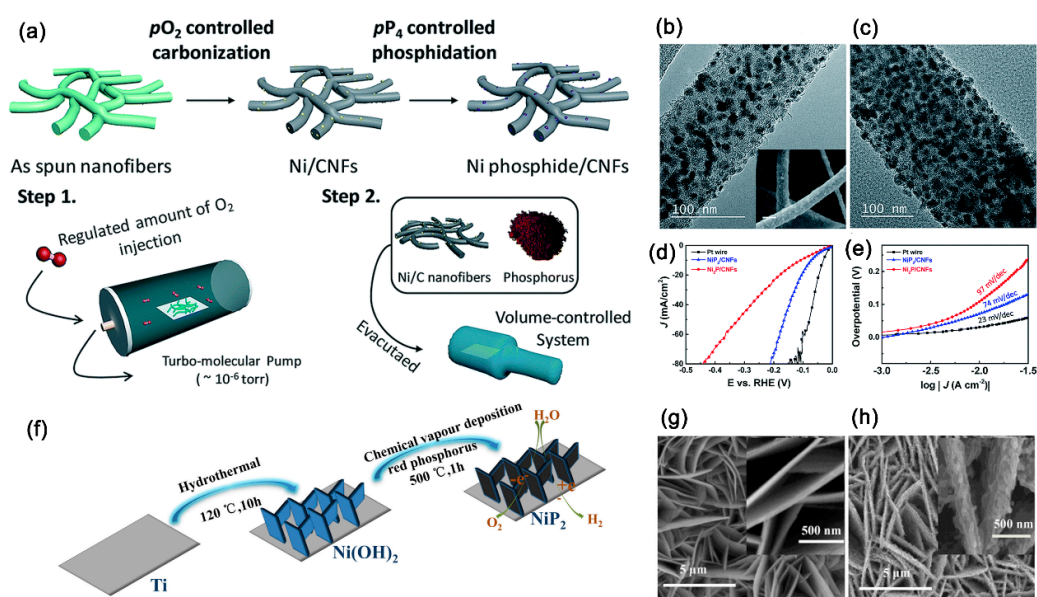

Figure 11. Schematic illustration for the overall synthesis of the Ni phosphide/CNFs (**a**). TEM (**b**) and SEM (insets) images of the Ni/CNFs-O_2 1.0 Torr, TEM image of the Ni phosphide/CNFs-O_2 1.0 Torr (**c**), Polarization curves (**d**), and Tafel plots (**e**) of the Ni_2P/CNFs, NiP_2/CNFs, and Pt wire. Reproduced with permission from Reference [51], Copyright the Royal Society of Chemistry, 2019. Schematic illustration of the experimental procedure used for NiP_2 synthesis (**f**), SEM images of $Ni(OH)_2$ (**g**), and NiP_2 (**h**) nanosheets on Ti foil. Reproduced with permission from Reference [49] Copyright Elsevier B.V., 2019.

Table 5. Summary of the nickel phosphide electrocatalysts prepared through thermal phosphidation with red phosphorus for HER in an acidic electrolyte.

Material and Morphology	Precursors [1]	Supports [2]	Loading mg/cm^2	Tafel Slope mV/dec	J mA/cm^2	η mV	Reference
Ni_3P microparticles	Ni powder	Ti plate	-	41 ± 2	10	66	[48]
Ni_2P nanosheet	$NiSO_4$	Ni foam	2	57	10	67	[122]
Ni_5P_4/Ni_2P/NiP_2 Nano-catalysts	$NiSO_4$ and $NiCl_2$	carbon fiber	25.8	58.8	10	98	[119]
Ni_5P_4 films	Ni foil	Ni foil	3.475	40	10	140	[113]
Ni_5P_4/Ni_2P nanosheet	Ni foam	Ni foam	68.2	79.1	10	120	[114]
Ni_5P_4-NiP_2 nanosheet	Ni foam	Ni foam	-	83.9	10	174	[116]
Ni_2P nanosheet	$Ni(NO_3)_2$	Ni foam	0.48	63	10	65	[121]
Ni_5P_4/NiP_2 nanoparticles	Ni foam and $Ni(NO_3)_2$	Ni foam	-	44	10	35	[118]
NiP_2 nanosheets	$Ni(NO_3)_2$	Ti foil	-	49.5	10	140	[49]
Ni_5P_4/NiP_2 nanosheets	Ni foam	Ni foam	39.3	52.8	10	92	[117]
Ni_2P nanoparticle	$NiSO_4$	Ti foils	-	84	100	163	[96]
Ni_2P nanoflakes	Ni foam	Ni foam	-	30	10	55	[123]
NiP_2 Nanofibers	$Ni(ac)_2$	GC	-	74	10	71	[51]
Ni/Ni_5P_4/NiP_2 nanosheets	Ni foam	Ni foam	-	51	10	61	[115]

[1] $Ni(ac)_2$: nickel acetate. [2] GC: glassy carbon.

Table 6. Summary of the nickel phosphide electrocatalysts prepared through thermal phosphidation with red phosphorus for HER in an alkaline electrolyte.

Material and Morphology	Precursors	Supports	Loading mg/cm^2	Tafel Slope mV/dec	J mA/cm^2	η mV	Reference
Ni$_3$P nanosheet	Ni powder	Ti plate	-	119 ± 2	10	291	[48]
Ni$_2$P nanosheet	NiSO$_4$	Ni foam	2	82	10	89	[122]
Ni$_5$P$_4$/Ni$_2$P/NiP$_2$ Nanocatalysts	NiSO$_4$ and NiCl$_2$	carbon fiber	25.8	85.4	10	117	[119]
Ni$_5$P$_4$ films	Ni foil	Ni foil	3.475	53	10	150	[113]
Ni$_2$P nanowires	Ni foam	Ni foam	-	-	100	224	[124]
NiP$_2$ nanosheets	Ni(NO$_3$)$_2$	Ti foil	-	60.5	10	134	[49]
Ni$_2$P nanoflakes	Ni foam	Ni foam	-	30	10	50	[123]

4.4. Hydrogen Reduction of Phosphates

Although highly crystallized nickel phosphide electrocatalysts with high HER performance can be prepared by thermal phosphidation with hypophosphite or red phosphorus, the PH$_3$ gas and P vapor generated during the process are relatively dangerous. Therefore, a safer and facile protocol that can produce highly crystallized nickel phosphide structures with high HER activity is still required. It is well known that hydrogen shows high reducibility under certain conditions. Thus, some researchers have employed hydrogen to reduce phosphates at a higher temperature to produce nickel phosphide structures. For example, Bai et al. demonstrated the preparation of novel peapod-like Ni$_2$P/C nanocomposites via a two-step process, which is schematically shown in Figure 12a [125]. They first prepared NiNH$_4$PO$_4$·H$_2$O nanorods via a facile hydrothermal method at 170 °C for 24 h. The morphology and crystal phase of the NiNH$_4$PO$_4$·H$_2$O nanorods can be clearly known through a SEM image (Figure 12b), XRD pattern (Figure 12c), and TEM image (Figure 12d,e). Subsequently, the crystalline NiNH$_4$PO$_4$·H$_2$O nanorods were converted to peapod-like Ni$_2$P/C nanocomposites by calcination under hydrogen at 700 °C for 200 min. Through the SEM image (Figure 12f), the XRD pattern (Figure 12g), and TEM image (Figure 12h,i), it can be clearly seen that the NiNH$_4$PO$_4$·H$_2$O nanorods have been successfully transformed into peapod-like Ni$_2$P/C nanocomposites after calcination. The Ni$_2$P/C nanocomposites showed excellent electrocatalytic HER activities in 0.5 M H$_2$SO$_4$ with a small overpotential of 87 mV to attain the current density of 10 mA/cm^2 and a notably low Tafel slope of 54 mV/dec (Figure 12j,k). The peapod-like Ni$_2$P/C nanocomposites can be used not only as an electrocatalytic hydrogen evolution reaction material, but also as an anode material for lithium-ion batteries. Then, by utilizing the similar approach, they successfully fabricated a novel 1-D peapod array of Ni$_2$P@graphitized carbon fiber composites on Ti foil substrate by hydrothermal growth and polymerization, which is followed by annealing in an H$_2$ atmosphere [126]. Miao et al. synthesized a core/shell structured chainmail catalyst of ultrathin P-doped carbon shell-encapsulated nickel phosphides on graphene through a facile solvothermal method following by an annealing treatment in hydrogen atmosphere, which exhibits remarkable electrocatalytic HER activities [127].
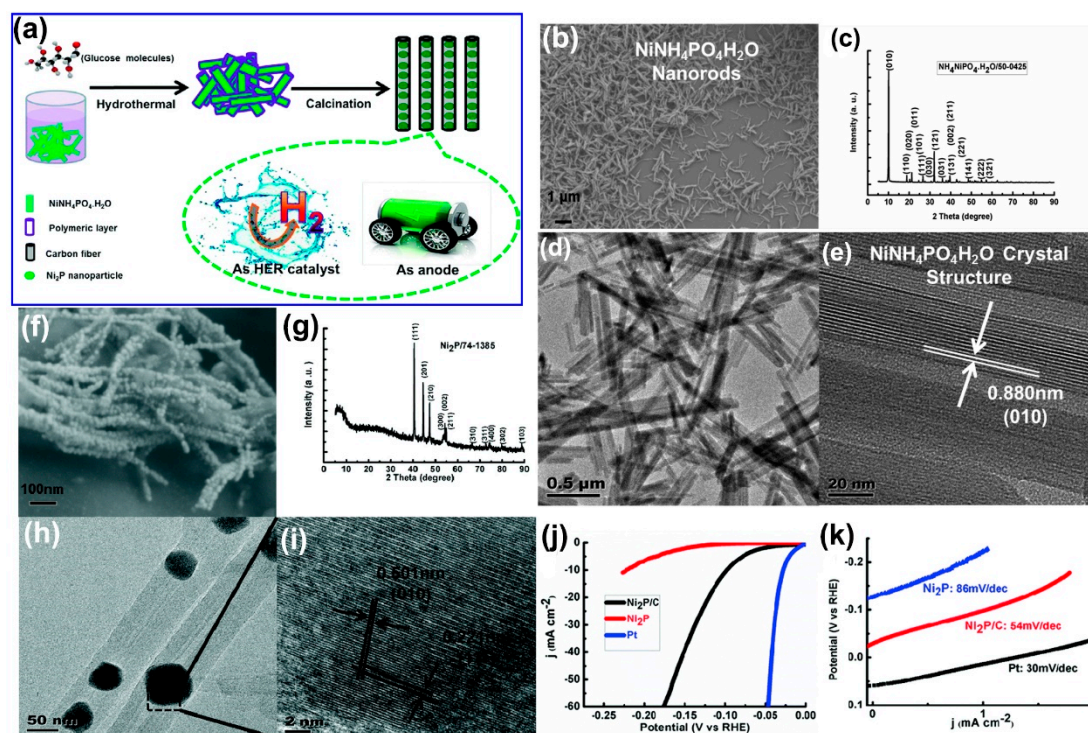
Figure 12. Schematic illustration of the synthetic procedure for the peapod-like Ni_2P/C nanocomposites (**a**), SEM image (**b**), XRD pattern (**c**), TEM (**d**), and HRTEM (**e**) images of $NiNH_4PO_4·H_2O$ nanorods. SEM image (**f**), XRD pattern (**g**), TEM (**h**), and HRTEM (**i**) images of Ni_2P/C composites. Polarization curves (**j**) and corresponding Tafel plots (**k**) for Ni_2P and Ni_2P/C electrodes in 0.5 M H_2SO_4. Reproduced with permission from Reference [127], Copyright The Royal Society of Chemistry, 2015.

The tunable compositions and hetero atom-enriched characteristics of inorganic−organic metal phosphonate hybrids make them promising templates and precursors to create high-performance nanomaterials as electrocatalysts for HER by high-temperature reduction. Lv et al. demonstrated the preparation of nitrogen-doped carbon-coated nickel phosphide nanoparticles on Ni foam by hydrogen reduction of the precursors of nickel phosphonates loaded on Ni foam [128]. Wang et al. reported the in-situ preparation of embedded ultrafine nickel phosphides in N-doped porous carbon nanofibers ($Ni_2P@NPCNFs$) by electrospinning the precursors, which is followed by a controllable pyrolyzed reduction in an H_2 atmosphere. The $Ni_2P@NPCNFs$ show excellent catalytic performance as an HER catalyst in acidic media, and good durability in neutral and basic media. This method was also demonstrated to prepare $Fe_2P@NPCNFs$, $Co_2P@NPCNFs$, and $Cu_3P@NPCNFs$ with the same nanostructure as $Ni_2P@NPCNFs$. This work provides a general approach for fabrication of transition metal phosphide structures with enhanced conductivity and catalytic activity. Table 7 summarizes the morphologies, mass loadings, and corresponding electrocatalytic HER performance in an acidic electrolyte of nickel phosphide electrocatalysts prepared through hydrogen reduction of phosphate precursors. As stated above, this hydrogen reduction of the phosphates method does not produce toxic or dangerous PH_3 gas or P vapor during the phosphidation process, and is very suitable for preparation of nickel phosphide electrocatalysts together with conductive supports (e.g., carbon). This is beneficial for the dispersion of the catalysts for high HER activities. However, it should also be noted that it is rather difficult to design or control the morphologies of the final nickel phosphides, and the process requires a relatively high temperature and involves explosive hydrogen gas.

Table 7. Summary of the nickel phosphide electrocatalysts prepared through hydrogen reduction of phosphates for HER in acidic electrolyte.

Material and Morphology	Precursors [1]	Middle Product	Supports [2]	Loading mg/cm^2	Tafel Slope mV/dec	J mA/cm^2	η mV	Reference
Ni$_2$P nanoparticles	Ni(NO$_3$)$_2$	NiNH$_4$PO$_4$	GC	0.36	54	10	87	[125]
Ni$_2$P nanoparticles	Ni(NO$_3$)$_2$	-	GC	0.51	58.6	10	110	[127]
Ni$_2$P peapods	Ni(NO$_3$)$_2$	NH$_4$NiPO$_4$	Ti foil	0.38	46	10	45	[126]
Ni$_2$P Nanoparticles	Ni(ac)$_2$	Nickel phosphonate powder	Ni foam	-	64	10	68	[128]
Ni$_2$P nanoparticles	NiSO$_4$	-	carbon cloth	0.337	56.7	10	63.2	[129]
Ni-Ni$_3$P nanoparticles	Ni(ac)$_2$	-	NPC/rGO	-	57.93	10	73	[130]

[1] Ni(ac)$_2$: nickel acetate. [2] GC: glassy carbon. NPC/rGO: N, P-doped carbon on 3D graphene frameworks.

4.5. Electrochemical Deposition

Electrochemical deposition, which involves the migration of the anions and cations in the electrolyte solution under an external electric field and the redox reactions on the electrode surfaces to deposit production layers, is recognized as a facile and mild preparation method due to the conditions generally at room temperature. Generally, it is difficult to obtain highly crystallized products and to control the morphologies through electrochemical deposition. For preparation of nickel phosphides, nickel and phosphorus alloys are generally produced by electrochemical deposition. In the preparation process, nickel-containing salts and phosphorus-containing salts are usually employed as precursors, and a conductive substrate is necessary to act as the electrode to support the depositions. So far, some interesting nickel phosphide structures have been successfully prepared by electrochemical deposition. Cao et al. demonstrated the preparation of hierarchical radial amorphous nickel phosphide (Ni$_x$P) nanospheres on Ni foam (Ni$_x$P/NF) at a constant potential of −0.8 V (vs. Ag/AgCl) under a nitrogen atmosphere by using a nickel chloride and sodium hypophosphite electrolyte [131]. Figure 13a shows a schematic image of the electrodeposition preparation of the hierarchical radial Ni$_x$P nanospheres on Ni foam at different times. The SEM images in Figure 13b,d together with the TEM images in Figure 13e,f,g clearly show the radial microstructure and morphology of the as-prepared Ni$_x$P nanospheres. The Ni$_x$P nanosphere has an amorphous phase and is composed of ultrathin nanosheets with a thickness of 8 nm near to the surface. The elemental mapping images in Figure 13h further verify the homogeneous distribution of Ni and P elements in Ni$_x$P nanospheres. The polarization curves in Figure 13i and Tafel plots in Figure 13j exhibit the electrocatalytic HER performance of the NixP nanospheres. Among them, the Ni$_x$P/NF-20 electrode exhibits the best HER performance in 1 M KOH solution with very low overpotential of 63 mV to achieve a current density of 10 mA/cm^2, and a Tafel slope as low as 55 mV/dec, which can be attributed to the 3D open-pore Ni foam structures with a high specific surface area and the high conductivity contributed by the in-situ deposition of highly ordered Ni$_x$P nanospheres on conductive Ni foam. Figure 13k illustrates the advantages of Ni$_x$P/NF-20 electrode during hydrogen evolution process in 1 M KOH, which follows the equation: $4e^- + 4H_2O \rightarrow 4OH^- + 2H_2$ [132]. Chen et al. reported the preparation of NiP$_x$ nanospheres on carbon cloth by cyclic voltammetry (CV) scanning between 0.2 V and −0.7 V (vs. NHE) at a scan rate of 50 mV/s by using nickel acetate (Ni(ac)$_2$) and sodium hypophosphite as precursors in acetate buffer solution (pH = 7) [133]. The NiP$_x$-coated carbon cloth electrode exhibits good HER performance in phosphate buffer saline (PBS) (pH = 7) solution. Similarly, Liu et al. deposited nickel–phosphorus nanoparticle films on Cu foam (Ni-P/CF) by CV scanning for 15 cycles between −1.0 and −0.3 V at a scan rate of 10 mV/s in electrolyte containing NiSO$_4$, KOH, and NaOAc [134]. The Ni-P/CF can deliver a current density of 10 mA/cm^2 at an overpotential of 98 mV for hydrogen production and 325 mV for oxygen generating in 1 M KOH solution. A two-electrode water electrolyzer using Ni-P/CF as cathode and anode produces 10 mA/cm^2 at a cell voltage of 1.68 V with high stability. Sun et al. prepared P-doped nickel (NiP$_x$) superstructure films on Cu foil by potentio-static deposition (PSD) and potentio-dynamic (PDD) approach, respectively [135]. By comparing the two deposition methods, it is found that the latter model with a potentio-dynamic

control is a valid electrochemical protocol to create crack-free NiP_x films. The PDD-NiP_x film shows a high HER activity under alkaline conditions. The PDD-Ni-10P achieved a low overpotential of 105 mV to deliver a current density of 10 mA/cm^2 with a small Tafel slope of 44.7 mV/dec and excellent catalytic stability for at least 60 h. Tang et al. reported the preparation of Ni-P alloy nanoparticle films on Ni foam by a linear voltammetry scan in the range of 1.2 to 0.2 V (vs. SCE) in the electrolyte solution of nickel sulfate, sodium hypophosphite, and sodium acetate [136]. The as-prepared Ni-P alloy nanoparticle film electrode can act as an efficient bifunctional water-splitting catalyst in strongly alkaline media, which drives 10 mA/cm^2 at overpotentials of 80 and 309 mV for HER and OER, respectively, and its two-electrode water electrolyzer needs a cell voltage of 1.67 V to achieve 10 mA/cm^2. Cheng et al. fabricated an Ni–P alloy on the plate via pulsed electrodeposition, and the Ni–P alloy with high capacitance performs the best HER catalytic activity [137]. In addition, Wu et al. fabricated self-supported Ni-P cathode by linear voltammetry scan from −0.3 to −0.9 V (vs Ag/AgCl) at a scan rate of 10 mV s^{-1} [138]. The Ni-P cathode performed a low onset over-potential, good catalytic activity, and long-term stability under neutral and alkaline conditions. The structural information, mass loading, and electrochemical HER performance in the alkaline electrolyte are summarized in Table 8 for comparison.
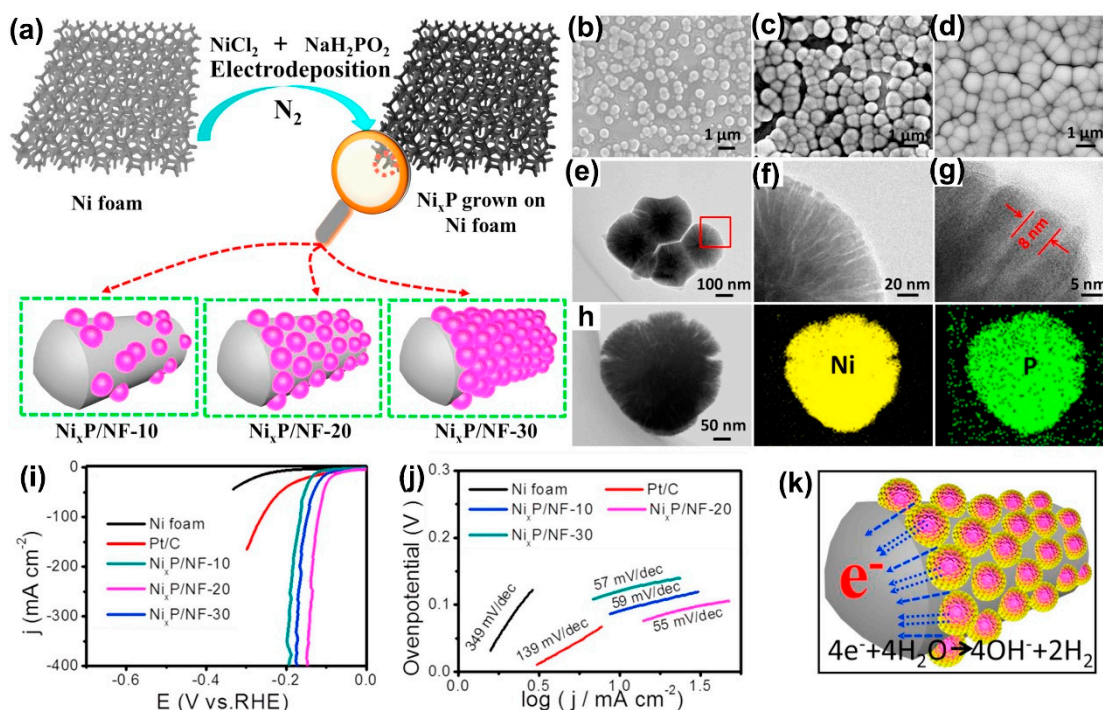

Figure 13. Schematic illustration for the electrochemical deposition of hierarchical radial Ni_xP nanospheres on Ni foam (**a**), SEM images of Ni_xP/NF-10 (**b**), Ni_xP/NF-20 (**c**), and Ni_xP/NF-30 (**d**), TEM image of radial Ni_xP-10 nanospheres (**e**), the magnified TEM image of a red squared indicated area (**f**), HRTEM (**g**), and elemental mapping images of the radial Ni_xP-10 nanospheres (**h**). iR-corrected LSV curves for Ni_xP/Ni foam, pristine Ni foam, and Pt/C electrodes for HER (**i**) and corresponding Tafel plots (**j**), and schematic illustration of the advantages of the brushy surface of Ni_xP/NF-20 for HER (**k**). Reproduced with permission from Reference [131], Copyright Elsevier B.V., 2018.

Table 8. Summary of the nickel phosphide electrocatalysts prepared through electrochemical deposition for HER.

Material and Morphology	Precursors [1]	Supports [2]	Electrolytes [3]	Loading mg/cm^2	Tafel Slope mV/dec	J mA/cm^2	η mV	Reference
NiP$_x$ films	NiCl$_2$	Cu foil	1M KOH	0.55	47.7	10	105	[135]
Ni$_x$P nanospheres	NiCl$_2$	Ni foam	1M KOH	4.4	55	10	63	[131]
Ni-P alloy Nanoparticle	NiSO$_4$	Ni foam	1M KOH	3.2	50	10	75	[136]
Ni-P nanoparticles film	NiSO$_4$	Cu foam	1M KOH	~5	55	10	98	[134]
Ni–P alloy	NiSO$_4$	Ni plate	1 M NaOH	3.85	59.7	10	134	[137]
Ni-Ni$_x$P nanospheres	NiSO$_4$	carbon cloth	0.5M H$_2$SO$_4$	-	76	10	164	[139]
Amorphous Ni-P film	NiSO$_4$	Cu sheet	0.5M H$_2$SO$_4$	-	54	10	222	[140]
Ni$_{78}$P$_{22}$ film	NiCl$_2$	Ti foil	0.5M H$_2$SO$_4$	-	38	10	105	[141]
Single-phase Ni$_5$P$_4$	NiCl$_2$	Cu foam	0.5M H$_2$SO$_4$	-	49	10	90	[142]
Ni$_x$P/CNT hybrid	NiSO$_4$	CNT	0.5M H$_2$SO$_4$	-	61.8	10	150	[143]
NiP$_x$ nanospheres	Ni(ac)$_2$	carbon cloth	0.1 M PBS (pH = 7)	0.235	101	10	230	[133]

[1] Ni(ac)$_2$: nickel acetate. [2] CNT: carbon nanotubes. [3] PBS: phosphate buffer saline.

Nickel phosphides prepared by the electrochemical deposition method also show remarkable HER activities in acidic solution. For instance, Ren et al. prepared nickel/nickel phosphide nanospheres electrode via in-situ reduction of NiSO$_4$ and NaH$_2$PO$_2$ on carbon cloth substrates using square-wave and CV methods, respectively [139]. It is found that nickel/nickel phosphide nanospheres prepared with the pulse deposition procedure exhibits higher HER performance than those prepared through the CV approach. As-prepared nickel/nickel phosphide/carbon cloth electrodes exhibit a cathodic current of 10 mA/cm^2 at the overpotential of 164 mV in a 0.5 M H$_2$SO$_4$ solution and a Tafel slope of 76 mV/dec. Wasalathanthri et al. prepared amorphous nickel phosphide thin films on Cu foil by electrodeposition at a constant current density of 10 mA/cm^2 for 10 min, which exhibits a good activity and long-term stability in acidic medium, with a potential of −222 mV to achieve 10 mA/cm^2 [140]. Wang et al. reported the preparation of amorphous sponge-like nickel phosphide-carbon nanotube (Ni$_x$P/CNT) hybrid electrodes through CV deposition [143]. These Ni$_x$P/CNTs exhibit superior catalytic activity for sustained hydrogen evolution in acidic, neutral, and basic media, which is attributed to the 3D porous nanoarchitecture consisting of a highly conductive 3D porous CNT backbone and a well-deposited Ni$_x$P nanoparticle catalyst. Apart from this, Kim et al. reported that pulse electrodeposition can be used to prepare an amorphous Ni-P catalyst with a high portion of P, which confers acid-resistant properties to the catalyst [141]. Most of the nickel phosphide catalysts prepared by electrodeposition are amorphous, but Das et al. fabricated copper foam @ single-phase Ni$_5$P$_4$ superhydrophilic and aerophobic core–shell nanostructures through a two-step process [142]. They first prepared a copper foam electrode by implementing a constant current density of 1 A/cm^2. Then, electrodeposition of Ni$_5$P$_4$ on copper foam was conducted by implementing a constant potential of −0.8 V. Figure 14a clearly shows the schematic image of the electrochemical synthesis of the copper foam @ Ni$_5$P$_4$ structures. The SEM images in Figure 14b,c indicate the microstructures and morphologies of the as-prepared Cu@Ni$_5$P$_4$. As shown in Figure 14d,e,f,g, the density functional theory (DFT) model, Ni$_5$P$_4$ (0001) and Ni$_5$P$_4$ (0001)/Cu (111) surface with H* adsorbed over the three-fold Ni site (site I) exhibited a negative value of DGH*, which favors HER activity. DFT calculations elucidated the origin of a very high negative DGH* in Ni$_5$P$_4$ (0001)/Cu (111) upon hydrogen adsorption. This arises due to a localized charge density distribution around the three-fold Ni site of the adsorbate, which is favorable for the HER activity of the catalyst. The super-hydrophilic and aero-phobic nanostructured surface also contributes to the HER performance by reducing the contact resistance and the fast release of air bubbles during the catalysis process. In order to evaluate the HER performance of the materials prepared by electrochemical deposition in an acidic solution, the structural information, mass loading, and electrochemical HER performance in an acidic electrolyte are also summarized in Table 8. It can be easily found that the electrochemical deposition method for preparation of nickel phosphides shows some apparent advantages such as mild preparation with no need of high temperature, low cost, and high safety with no toxic chemicals. However, there are still some weakness of this method. For

instance, it is difficult to control the morphologies and the products are generally amorphous, which may limit the intrinsic activities. Therefore, efforts are still required to address the above issues to obtain stable and highly crystallized nickel phosphide electrocatalysts with high HER activities.
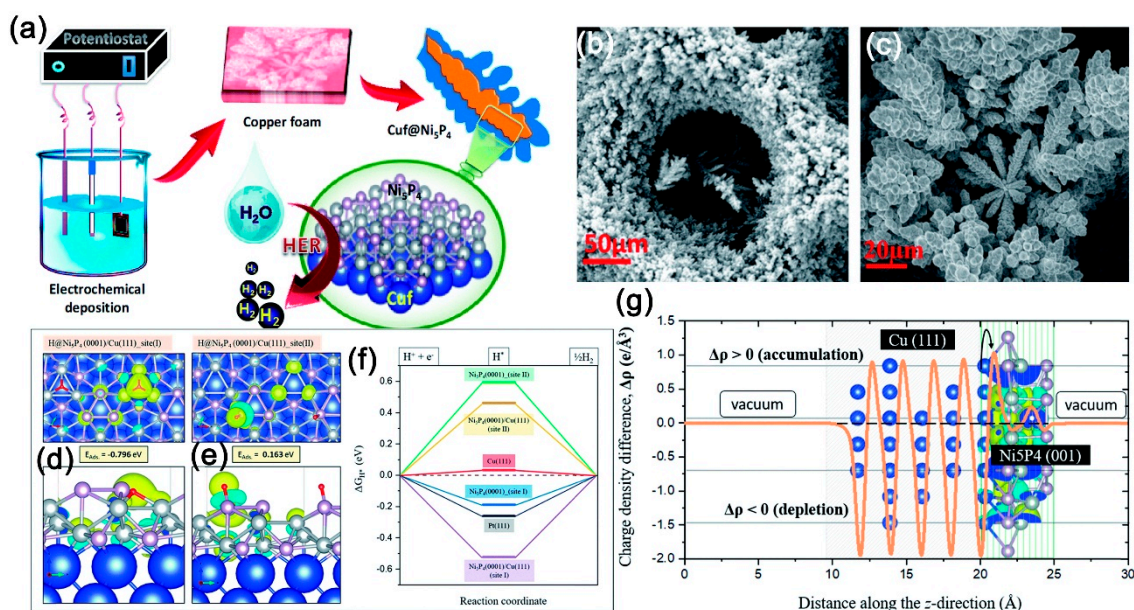

Figure 14. Schematic illustration of the electrochemical synthesis of nickel phosphides on Cu foam (**a**), SEM images of the Ni_5P_4 on Cu foam (**b**,**c**), top and side view of H* adsorption over the three-fold Ni site of the Ni_5P_4 (0001)/Cu (111) (site I) (**d**), and H* over the on-top P site of the Ni_5P_4 (0001)/Cu (111) surface (site II) (**e**). The differential ground state charge density distribution around the adsorbate (H*) is at an iso-level of 0.59×10^{-2} eÅ^{-3}. The ΔG_{H*} of the reaction intermediate (H*) on different metal-catalyst surfaces (**f**) and charge density difference and charge transfer at the interface between Cu (111) and Ni_5P_4 (001) surface (**g**). Reproduced with permission from Reference [142], Copyright The Royal Society of Chemistry, 2019.

5. Conclusions and Perspectives

In this review, we have comprehensively summarized the progresses of nickel phosphide electrocatalysts for a hydrogen evolution reaction based on the preparation approaches. There are five main protocols, i.e., solution-phase synthesis, thermal phosphidation with hypophosphite, thermal phosphidation with red phosphorus, hydrogen reduction of phosphates, and electrochemical deposition method, to fabricate nickel phosphide structures in which the advantages and weakness are discussed in the article and also summarized in Table 9. The morphologies and HER performances of nickel phosphide electrocatalysts prepared by each approach are discussed and compared in detail, which suggest that the nickel phosphide structures prepared through thermal phosphidation with hypophosphite or red phosphorus exhibit higher HER activities. The thermal phosphidation methods show versatility on the control of the structures and morphologies. Notably, the solution-phase approach is suitable for preparation of nickel phosphide catalysts ink, which is compatible with printing technologies to produce membrane electrodes, even though this method has a relatively high cost.

Table 9. Comparison of the preparation methods of nickel phosphide electrocatalysts for HER.

Methods	Advantages	Disadvantages
Solution-phase method	Easy to fabricate nickel phosphide nanoparticles with small size and high surface area, compatible with the printing technologies for membrane electrodes	High cost and toxicity of the organic phosphine, relatively complicated post process after the reaction, difficult to control structures and morphologies of the products
Thermal phosphidation with hypophosphite	Easy to control the morphologies by controlling the morphologies of pre-prepared Ni precursors, easy fabrication on conductive supports as electrodes	Toxic PH$_3$ generated in the phosphidation process
Thermal phosphidation with red phosphorus	Relatively high safety, easy to control the morphologies by controlling the pre-prepared Ni precursors, easy fabrication on conductive supports as electrodes	Precursors mainly based on metallic nickel materials
Hydrogen reduction of phosphates	Relatively high safety, easy preparation of nickel phosphides, relatively low cost, relatively large scale	Difficult to control the structures and morphologies of the final nickel phosphides
Electrochemical deposition	Mild preparation, low cost, high safety	Generally amorphous phase, mainly forming Ni-P alloy, particularly difficult to control the structures and morphologies of the nickel phosphides, relatively inferior HER activities, preparation only on conductive electrodes

The HER activities, high conductivity, and high physicochemical stability endow nickel phosphides with outstanding HER performances, especially in an acidic electrolyte, which have gone beyond the state-of-the-art transition metal sulfide catalysts. However, challenges still exist for next-generation HER electrocatalysts based on nickel phosphides. First, it is urgently necessary to deeply understand the active sites of nickel phosphide or other transition metal phosphide electrocatalysts toward the HER reaction, especially the catalytic process (i.e., hydrogen adsorption, diffusion, and combination) on the surfaces. The influence of the nickel phosphide crystal phase on HER activity is still not fully understood, even though some studies have involved such issues. Further studies are required to elucidate the relationship between the HER activity and a specific facet of nickel phosphides, as well as the relationship between HER activity and the stoichiometry of Ni and P. Second, to date, the intrinsic electrocatalytic HER activity of nickel phosphides is still too low for practical applications. Some studies reported high-performance HER electrocatalysts based on nickel phosphide structures, but the mass loading is too high, which remarkably reduces the competitiveness with noble Pt-based catalysts in practical use. Fortunately, researchers have recognized that heteroatomic doping or defect engineering, which allow structural modulation at the lattice level is effective to improve the intrinsic electrocatalytic HER activity of nickel phosphides through the synergistic effect. Third, the exposure of sufficient active sites is required to improve the comprehensive HER performance, which is critical for practical applications. Generally, the construction of hierarchical or porous structures with a high surface area and optimized pore size distribution is carried out to maximize the effective active surface area to participate in the electrocatalytic reactions. However, current results still hardly satisfy the demand due to the loss of activities at most of the exposure sites, even though some beautiful hierarchical or porous structures with high electrochemical surface areas have been developed. Therefore, principle studies focusing on the dependence of HER activities on the crystal phase, crystal facet, compositions, doping, and defects by combining experiments and theoretical simulation, which elucidate the origins of the high activity and the possible synergistic effects, may provide a fundamental instruction for rational design and construction of next generation electrocatalysts based on nickel phosphides for hydrogen production.

Conflicts of Interest: The authors declare no conflict of interest.

References

1. Turner, J.A. Sustainable Hydrogen Production. *Science* **2004**, *305*, 972. [CrossRef] [PubMed]

2. Caban-Acevedo, M.; Stone, M.L.; Schmidt, J.R.; Thomas, J.G.; Ding, Q.; Chang, H.-C.; Tsai, M.-L.; He, J.-H.; Jin, S. Efficient hydrogen evolution catalysis using ternary pyrite-type cobalt phosphosulphide. *Nat. Mater.* **2015**, *14*, 1245–1251. [CrossRef] [PubMed]

3. Le Goff, A.; Artero, V.; Jousselme, B.; Tran, P.D.; Guillet, N.; Métayé, R.; Fihri, A.; Palacin, S.; Fontecave, M. From Hydrogenases to Noble Metal–Free Catalytic Nanomaterials for H_2 Production and Uptake. *Science* **2009**, *326*, 1384. [CrossRef] [PubMed]

4. Luo, J.; Im, J.-H.; Mayer, M.T.; Schreier, M.; Nazeeruddin, M.K.; Park, N.-G.; Tilley, S.D.; Fan, H.J.; Grätzel, M. Water photolysis at 12.3% efficiency via perovskite photovoltaics and Earth-abundant catalysts. *Science* **2014**, *345*, 1593. [CrossRef]

5. Hellstern, T.R.; Benck, J.D.; Kibsgaard, J.; Hahn, C.; Jaramillo, T.F. Engineering Cobalt Phosphide (CoP) Thin Film Catalysts for Enhanced Hydrogen Evolution Activity on Silicon Photocathodes. *Adv. Energy Mater.* **2016**, *6*, 1501758. [CrossRef]

6. Anantharaj, S.; Ede, S.R.; Sakthikumar, K.; Karthick, K.; Mishra, S.; Kundu, S. Recent Trends and Perspectives in Electrochemical Water Splitting with an Emphasis on Sulfide, Selenide, and Phosphide Catalysts of Fe, Co, and Ni: A Review. *ACS Catal.* **2016**, *6*, 8069–8097. [CrossRef]

7. Li, A.; Sun, Y.; Yao, T.; Han, H. Earth-Abundant Transition-Metal-Based Electrocatalysts for Water Electrolysis to Produce Renewable Hydrogen. *Chem.-Eur. J.* **2018**, *24*, 18334–18355. [CrossRef]

8. McKone, J.R.; Marinescu, S.C.; Brunschwig, B.S.; Winkler, J.R.; Gray, H.B. Earth-abundant hydrogen evolution electrocatalysts. *Chem. Sci.* **2014**, *5*, 865–878. [CrossRef]

9. Ledendecker, M.; Schlott, H.; Antonietti, M.; Meyer, B.; Shalom, M. Experimental and Theoretical Assessment of Ni-Based Binary Compounds for the Hydrogen Evolution Reaction. *Adv. Energy Mater.* **2016**, *7*, 1601735. [CrossRef]

10. Vij, V.; Sultan, S.; Harzandi, A.M.; Meena, A.; Tiwari, J.N.; Lee, W.-G.; Yoon, T.; Kim, K.S. Nickel-Based Electrocatalysts for Energy-Related Applications: Oxygen Reduction, Oxygen Evolution, and Hydrogen Evolution Reactions. *ACS Catal.* **2017**, *7*, 7196–7225. [CrossRef]

11. Abbas, M.A.; Bang, J.H. Rising Again: Opportunities and Challenges for Platinum-Free Electrocatalysts. *Chem. Mater.* **2015**, *27*, 7218–7235. [CrossRef]

12. Chen, Z.; Shan, A.; Cui, Y.; Wang, R.; Chen, C. Catalysis of hydrogen evolution reaction by $Ni_{12}P_5$ single crystalline nanoplates and spherical nanoparticles. *CrystEngComm* **2019**, *21*, 228–235. [CrossRef]

13. Gong, M.; Dai, H. A mini review of NiFe-based materials as highly active oxygen evolution reaction electrocatalysts. *Nano Res.* **2015**, *8*, 23–39. [CrossRef]

14. Han, L.; Dong, S.; Wang, E. Transition-Metal (Co, Ni, and Fe)-Based Electrocatalysts for the Water Oxidation Reaction. *Adv. Mater.* **2016**, *28*, 9266–9291. [CrossRef]

15. Kim, J.S.; Kim, B.; Kim, H.; Kang, K. Recent Progress on Multimetal Oxide Catalysts for the Oxygen Evolution Reaction. *Adv. Energy Mater.* **2018**, *8*, 1702774. [CrossRef]

16. Li, D.; Shi, J.; Li, C. Transition-Metal-Based Electrocatalysts as Cocatalysts for Photoelectrochemical Water Splitting: A Mini Review. *Small* **2018**, *14*, 1704179. [CrossRef]

17. Owens-Baird, B.; Kolen'ko, Y.V.; Kovnir, K. Structure–Activity Relationships for Pt-Free Metal Phosphide Hydrogen Evolution Electrocatalysts. *Chem.-Eur. J.* **2018**, *24*, 7298–7311. [CrossRef]

18. Pei, Y.; Cheng, Y.; Chen, J.; Smith, W.; Dong, P.; Ajayan, P.M.; Ye, M.; Shen, J. Recent developments of transition metal phosphides as catalysts in the energy conversion field. *J. Mater. Chem. A* **2018**, *6*, 23220–23243. [CrossRef]

19. Tareen, A.K.; Priyanga, G.S.; Khan, K.; Pervaiz, E.; Thomas, T.; Yang, M. Nickel-Based Transition Metal Nitride Electrocatalysts for the Oxygen Evolution Reaction. *ChemSusChem* **2019**, *12*, 3941–3954. [CrossRef]

20. Liu, X.; Chi, J.; Dong, B.; Sun, Y. Recent Progress in Decoupled H$_2$ and O$_2$ Production from Electrolytic Water Splitting. *ChemElectroChem* **2019**, *6*, 2157–2166. [CrossRef]

21. Xiao, P.; Chen, W.; Wang, X. A Review of Phosphide-Based Materials for Electrocatalytic Hydrogen Evolution. *Adv. Energy Mater.* **2015**, *5*, 1500985. [CrossRef]

22. Roger, I.; Symes, M.D. First row transition metal catalysts for solar-driven water oxidation produced by electrodeposition. *J. Mater. Chem. A* **2016**, *4*, 6724–6741. [CrossRef]

23. McCrory, C.C.L.; Jung, S.; Ferrer, I.M.; Chatman, S.M.; Peters, J.C.; Jaramillo, T.F. Benchmarking Hydrogen Evolving Reaction and Oxygen Evolving Reaction Electrocatalysts for Solar Water Splitting Devices. *J. Am. Chem. Soc.* **2015**, *137*, 4347–4357. [CrossRef]

24. McCrory, C.C.L.; Jung, S.; Peters, J.C.; Jaramillo, T.F. Benchmarking Heterogeneous Electrocatalysts for the Oxygen Evolution Reaction. *J. Am. Chem. Soc.* **2013**, *135*, 16977–16987. [CrossRef]

25. Manzanares Palenzuela, C.L.; Luxa, J.; Sofer, Z.; Pumera, M. MoSe$_2$ Dispersed in Stabilizing Surfactant Media: Effect of the Surfactant Type and Concentration on Electron Transfer and Catalytic Properties. *ACS Appl. Mater. Interfaces* **2018**, *10*, 17820–17826. [CrossRef]

26. Burke, M.S.; Zou, S.; Enman, L.J.; Kellon, J.E.; Gabor, C.A.; Pledger, E.; Boettcher, S.W. Revised Oxygen Evolution Reaction Activity Trends for First-Row Transition-Metal (Oxy)hydroxides in Alkaline Media. *J. Phys. Chem. Lett.* **2015**, *6*, 3737–3742. [CrossRef]

27. Browne, M.P.; Sofer, Z.; Pumera, M. Layered and two dimensional metal oxides for electrochemical energy conversion. *Energy Environ. Sci.* **2019**, *12*, 41–58. [CrossRef]

28. Lyons, M.E.G.; Doyle, R.L.; Fernandez, D.; Godwin, I.J.; Browne, M.P.; Rovetta, A. The mechanism and kinetics of electrochemical water oxidation at oxidized metal and metal oxide electrodes. Part 1. General considerations: A mini review. *Electrochem. Commun.* **2014**, *45*, 60–62. [CrossRef]

29. Walter, M.G.; Warren, E.L.; McKone, J.R.; Boettcher, S.W.; Mi, Q.; Santori, E.A.; Lewis, N.S. Solar Water Splitting Cells. *Chem. Rev.* **2010**, *110*, 6446–6473. [CrossRef]

30. Conway, B.E.; Tilak, B.V. Interfacial processes involving electrocatalytic evolution and oxidation of H$_2$, and the role of chemisorbed H. *Electrochim. Acta* **2002**, *47*, 3571–3594. [CrossRef]

31. Li, Y.; Wang, H.; Xie, L.; Liang, Y.; Hong, G.; Dai, H. MoS2 Nanoparticles Grown on Graphene: An Advanced Catalyst for the Hydrogen Evolution Reaction. *J. Am. Chem. Soc.* **2011**, *133*, 7296–7299. [CrossRef] [PubMed]

32. Sultan, S.; Tiwari, J.N.; Singh, A.N.; Zhumagali, S.; Ha, M.; Myung, C.W.; Thangavel, P.; Kim, K.S. Single Atoms and Clusters Based Nanomaterials for Hydrogen Evolution, Oxygen Evolution Reactions, and Full Water Splitting. *Adv. Energy Mater.* **2019**, *9*, 1900624. [CrossRef]

33. Wang, J.; Xu, F.; Jin, H.; Chen, Y.; Wang, Y. Non-Noble Metal-based Carbon Composites in Hydrogen Evolution Reaction: Fundamentals to Applications. *Adv. Mater.* **2017**, *29*, 1605838. [CrossRef] [PubMed]

34. Fang, M.; Dong, G.; Wei, R.; Ho, J.C. Hierarchical Nanostructures: Design for Sustainable Water Splitting. *Adv. Energy Mater.* **2017**, *7*, 1700559. [CrossRef]

35. Yu, X.; Zhao, J.; Zheng, L.-R.; Tong, Y.; Zhang, M.; Xu, G.; Li, C.; Ma, J.; Shi, G. Hydrogen Evolution Reaction in Alkaline Media: Alpha- or Beta-Nickel Hydroxide on the Surface of Platinum? *ACS Energy Lett.* **2018**, *3*, 237–244. [CrossRef]

36. Prins, R.; De Beer, V.H.J.; Somorjai, G.A. Structure and Function of the Catalyst and the Promoter in Co—Mo Hydrodesulfurization Catalysts. *Catal. Rev.* **1989**, *31*, 1–41. [CrossRef]

37. Merki, D.; Hu, X. Recent developments of molybdenum and tungsten sulfides as hydrogen evolution catalysts. *Energy Environ. Sci.* **2011**, *4*, 3878–3888. [CrossRef]

38. Liu, P.; Rodriguez, J.A.; Asakura, T.; Gomes, J.; Nakamura, K. Desulfurization Reactions on Ni$_2$P(001) and α-Mo2C(001) Surfaces: Complex Role of P and C Sites. *J. Phys. Chem. B* **2005**, *109*, 4575–4583. [CrossRef]

39. Liu, P.; Rodriguez, J.A. Catalysts for hydrogen evolution from the NiFe hydrogenase to the Ni$_2$P(001) surface: The importance of ensemble effect. *J. Am. Chem. Soc.* **2005**, *127*, 14871–14878. [CrossRef]

40. Rundqvist, S.; Yhland, M.; Dahlbom, R.; Sjövall, J.; Theander, O.; Flood, H. X-Ray Investigations of Mn$_3$P, Mn$_2$P, and Ni$_2$P. *Acta Chem. Scand.* **1962**, *16*, 992–998. [CrossRef]

41. Prins, R.; Bussell, M.E. Metal Phosphides: Preparation, Characterization and Catalytic Reactivity. *Catal. Lett.* **2012**, *142*, 1413–1436. [CrossRef]

42. Oyama, S.T. Novel catalysts for advanced hydroprocessing: Transition metal phosphides. *J. Catal.* **2003**, *216*, 343–352. [CrossRef]

43. Sawhill, S.J.; Phillips, D.C.; Bussell, M.E. Thiophene hydrodesulfurization over supported nickel phosphide catalysts. *J. Catal.* **2003**, *215*, 208–219. [CrossRef]

44. Layman, K.A.; Bussell, M.E. Infrared Spectroscopic Investigation of Thiophene Adsorption on Silica-Supported Nickel Phosphide Catalysts. *J. Phys. Chem. B* **2004**, *108*, 15791–15802.

45. Popczun, E.J.; McKone, J.R.; Read, C.G.; Biacchi, A.J.; Wiltrout, A.M.; Lewis, N.S.; Schaak, R.E. Nanostructured Nickel Phosphide as an Electrocatalyst for the Hydrogen Evolution Reaction. *J. Am. Chem. Soc.* **2013**, *135*, 9267–9270.

46. Lai, C.; Liu, X.; Deng, Y.; Yang, H.; Jiang, H.; Xiao, Z.; Liang, T. Rice-shape nanocrystalline Ni_5P_4: A promising bifunctional electrocatalyst for hydrogen evolution reaction and oxygen evolution reaction. *Inorg. Chem. Commun.* **2018**, *97*, 98–102. [CrossRef]

47. Wang, C.; Ding, T.; Sun, Y.; Zhou, X.; Liu, Y.; Yang, Q. $Ni_{12}P_5$ nanoparticles decorated on carbon nanotubes with enhanced electrocatalytic and lithium storage properties. *Nanoscale* **2015**, *7*, 19241–19249. [CrossRef]

48. Laursen, A.B.; Wexler, R.B.; Whitaker, M.J.; Izett, E.J.; Calvinho, K.U.D.; Hwang, S.; Rucker, R.; Wang, H.; Ji, J.; Garfunkel, E.; et al. Climbing the Volcano of Electrocatalytic Activity while Avoiding Catalyst Corrosion: Ni_3P, a Hydrogen Evolution Electrocatalyst Stable in Both Acid and Alkali. *ACS Catal.* **2018**, *8*, 4408–4419. [CrossRef]

49. Cao, Q.; Wang, C.; Chen, S.; Xu, X.; Liu, F.; Geng, X.; Wang, J. Vertically aligned NiP_2 nanosheets with interlaced mesh network for highly efficient water splitting under alkaline and acid solutions. *Int. J. Hydrog. Energ.* **2019**, *44*, 6535–6543. [CrossRef]

50. Pan, Y.; Liu, Y.; Zhao, J.; Yang, K.; Liang, J.; Liu, D.; Hu, W.; Liu, D.; Liu, Y.; Liu, C. Monodispersed nickel phosphide nanocrystals with different phases: Synthesis, characterization and electrocatalytic properties for hydrogen evolution. *J. Mater. Chem. A* **2015**, *3*, 1656–1665. [CrossRef]

51. Kim, J.-Y.; Park, H.; Joo, W.; Nam, D.-H.; Lee, S.; Kim, H.G.; Ahn, I.-K.; Kang, H.-Y.; Lee, G.-B.; Jung, I.-h.; et al. Predictive fabrication of Ni phosphide embedded in carbon nanofibers as active and stable electrocatalysts. *J. Mater. Chem. A* **2019**, *7*, 7451–7458.

52. Moon, J.-S.; Jang, J.-H.; Kim, E.-G.; Chung, Y.-H.; Yoo, S.J.; Lee, Y.-K. The nature of active sites of Ni_2P electrocatalyst for hydrogen evolution reaction. *J. Catal.* **2015**, *326*, 92–99. [CrossRef]

53. Li, Y.; Cai, P.; Ci, S.; Wen, Z. Strongly Coupled 3D Nanohybrids with Ni_2P/Carbon Nanosheets as pH-Universal Hydrogen Evolution Reaction Electrocatalysts. *ChemElectroChem* **2017**, *4*, 340–344.

54. Li, H.; Wang, W.; Gong, Z.; Yu, Y.; Piao, l.; Chen, H.; Xia, J. Shape-controlled synthesis of nickel phosphide nanocrystals and their application as hydrogen evolution reaction catalyst. *J. Phys. Chem. Solids* **2015**, *80*, 22–25. [CrossRef]

55. Pan, Y.; Lin, Y.; Liu, Y.; Liu, C. Size-dependent magnetic and electrocatalytic properties of nickel phosphide nanoparticles. *Appl. Surf. Sci.* **2016**, *366*, 439–447. [CrossRef]

56. Zhang, C.; Xin, B.; Xi, Z.; Zhang, B.; Li, Z.; Zhang, H.; Li, Z.; Hao, J. Phosphonium-Based Ionic Liquid: A New Phosphorus Source toward Microwave-Driven Synthesis of Nickel Phosphide for Efficient Hydrogen Evolution Reaction. *ACS Sustain. Chem. Eng.* **2018**, *6*, 1468–1477. [CrossRef]

57. Wang, X.; Kolen'ko, Y.V.; Liu, L. Direct solvothermal phosphorization of nickel foam to fabricate integrated Ni_2P-nanorods/Ni electrodes for efficient electrocatalytic hydrogen evolution. *Chem. Commun.* **2015**, *51*, 6738–6741. [CrossRef]

58. Yu, J.; Li, Q.; Chen, N.; Xu, C.-Y.; Zhen, L.; Wu, J.; Dravid, V.P. Carbon-Coated Nickel Phosphide Nanosheets as Efficient Dual-Electrocatalyst for Overall Water Splitting. *ACS Appl. Mater. Interfaces* **2016**, *8*, 27850–27858. [CrossRef]

59. Shi, Y.; Xu, Y.; Zhuo, S.; Zhang, J.; Zhang, B. Ni_2P Nanosheets/Ni Foam Composite Electrode for Long-Lived and pH-Tolerable Electrochemical Hydrogen Generation. *ACS Appl. Mater. Interfaces* **2015**, *7*, 2376–2384.

60. Roberts, E.J.; Read, C.G.; Lewis, N.S.; Brutchey, R.L. Phase Directing Ability of an Ionic Liquid Solvent for the Synthesis of HER-Active Ni_2P Nanocrystals. *ACS Appl. Energy Mater.* **2018**, *1*, 1823–1827.

61. Huang, Z.; Chen, Z.; Chen, Z.; Lv, C.; Meng, H.; Zhang, C. $Ni_{12}P_5$ Nanoparticles as an Efficient Catalyst for Hydrogen Generation via Electrolysis and Photoelectrolysis. *ACS Nano* **2014**, *8*, 8121–8129. [CrossRef]

62. Lin, Y.; Zhang, J.; Pan, Y.; Liu, Y. Nickel phosphide nanoparticles decorated nitrogen and phosphorus co-doped porous carbon as efficient hybrid catalyst for hydrogen evolution. *Appl. Surf. Sci.* **2017**, *422*, 828–837. [CrossRef]

63. Li, H.; Lu, S.; Sun, J.; Pei, J.; Liu, D.; Xue, Y.; Mao, J.; Zhu, W.; Zhuang, Z. Phase-Controlled Synthesis of Nickel Phosphide Nanocrystals and Their Electrocatalytic Performance for the Hydrogen Evolution Reaction. *Chem.-Eur. J.* **2018**, *24*, 11748–11754. [CrossRef]

64. Seo, B.; Baek, D.S.; Sa, Y.J.; Joo, S.H. Shape effects of nickel phosphide nanocrystals on hydrogen evolution reaction. *CrystEngComm* **2016**, *18*, 6083–6089. [CrossRef]

65. Laursen, A.B.; Patraju, K.R.; Whitaker, M.J.; Retuerto, M.; Sarkar, T.; Yao, N.; Ramanujachary, K.V.; Greenblatt, M.; Dismukes, G.C. Nanocrystalline Ni_5P_4: A hydrogen evolution electrocatalyst of exceptional efficiency in both alkaline and acidic media. *Energy Environ. Sci.* **2015**, *8*, 1027–1034. [CrossRef]

66. Lin, Y.; Pan, Y.; Zhang, J. In-situ grown of Ni_2P nanoparticles on 2D black phosphorus as a novel hybrid catalyst for hydrogen evolution. *Int. J. Hydrog. Energ.* **2017**, *42*, 7951–7956. [CrossRef]

67. Chang, J.; Li, S.; Li, G.; Ge, J.; Liu, C.; Xing, W. Monocrystalline $Ni_{12}P_5$ hollow spheres with ultrahigh specific surface areas as advanced electrocatalysts for the hydrogen evolution reaction. *J. Mater. Chem. A* **2016**, *4*, 9755–9759. [CrossRef]

68. Jin, L.; Xia, H.; Huang, Z.; Lv, C.; Wang, J.; Humphrey, M.G.; Zhang, C. Phase separation synthesis of trinickel monophosphide porous hollow nanospheres for efficient hydrogen evolution. *J. Mater. Chem. A* **2016**, *4*, 10925–10932. [CrossRef]

69. Pan, Y.; Liu, Y.; Liu, C. Nanostructured nickel phosphide supported on carbon nanospheres: Synthesis and application as an efficient electrocatalyst for hydrogen evolution. *J. Power Sources* **2015**, *285*, 169–177. [CrossRef]

70. Pan, Y.; Yang, N.; Chen, Y.; Lin, Y.; Li, Y.; Liu, Y.; Liu, C. Nickel phosphide nanoparticles-nitrogen-doped graphene hybrid as an efficient catalyst for enhanced hydrogen evolution activity. *J. Power Sources* **2015**, *297*, 45–52. [CrossRef]

71. Chung, Y.-H.; Gupta, K.; Jang, J.-H.; Park, H.S.; Jang, I.; Jang, J.H.; Lee, Y.-K.; Lee, S.-C.; Yoo, S.J. Rationalization of electrocatalysis of nickel phosphide nanowires for efficient hydrogen production. *Nano Energy* **2016**, *26*, 496–503. [CrossRef]

72. Hansen, M.H.; Stern, L.-A.; Feng, L.; Rossmeisl, J.; Hu, X. Widely available active sites on Ni_2P for electrochemical hydrogen evolution – insights from first principles calculations. *Phys. Chem. Chem. Phys.* **2015**, *17*, 10823–10829. [CrossRef]

73. Surendran, S.; Shanmugapriya, S.; Shanmugam, S.; Vasylechko, L.; Kalai Selvan, R. Interweaved Nickel Phosphide Sponge as an Electrode for Flexible Supercapattery and Water Splitting Applications. *ACS Appl. Energy Mater.* **2018**, *1*, 78–92. [CrossRef]

74. Menezes, P.W.; Indra, A.; Das, C.; Walter, C.; Göbel, C.; Gutkin, V.; Schmeiβer, D.; Driess, M. Uncovering the Nature of Active Species of Nickel Phosphide Catalysts in High-Performance Electrochemical Overall Water Splitting. *ACS Catal.* **2017**, *7*, 103–109. [CrossRef]

75. Sun, H.; Xu, X.; Yan, Z.; Chen, X.; Cheng, F.; Weiss, P.S.; Chen, J. Porous Multishelled Ni_2P Hollow Microspheres as an Active Electrocatalyst for Hydrogen and Oxygen Evolution. *Chem. Mater.* **2017**, *29*, 8539–8547. [CrossRef]

76. Jiang, P.; Liu, Q.; Sun, X. NiP_2 nanosheet arrays supported on carbon cloth: An efficient 3D hydrogen evolution cathode in both acidic and alkaline solutions. *Nanoscale* **2014**, *6*, 13440–13445. [CrossRef]

77. Zheng, H.; Huang, X.; Wu, Z.; Gao, H.; Dong, W.; Wang, G. Controlled Synthesis of 3D Flower-like $Ni2P$ Composed of Mesoporous Nanoplates for Overall Water Splitting. *Chem.-Asian J.* **2017**, *12*, 2956–2961. [CrossRef]

78. Wang, H.; Xie, Y.; Cao, H.; Li, Y.; Li, L.; Xu, Z.; Wang, X.; Xiong, N.; Pan, K. Flower-Like Nickel Phosphide Microballs Assembled by Nanoplates with Exposed High-Energy (001) Facets: Efficient Electrocatalyst for the Hydrogen Evolution Reaction. *Chemsuschem* **2017**, *10*, 4899–4908. [CrossRef]

79. Li, J.; Li, J.; Zhou, X.; Xia, Z.; Gao, W.; Ma, Y.; Qu, Y. Highly Efficient and Robust Nickel Phosphides as Bifunctional Electrocatalysts for Overall Water-Splitting. *ACS Appl. Mater. Interfaces* **2016**, *8*, 10826–10834. [CrossRef]

80. Wang, X.-D.; Cao, Y.; Teng, Y.; Chen, H.-Y.; Xu, Y.-F.; Kuang, D.-B. Large-Area Synthesis of a Ni_2P Honeycomb Electrode for Highly Efficient Water Splitting. *ACS Appl. Mater. Interfaces* **2017**, *9*, 32812–32819. [CrossRef]

81. Yan, L.; Dai, P.; Wang, Y.; Gu, X.; Li, L.; Cao, L.; Zhao, X. In Situ Synthesis Strategy for Hierarchically Porous Ni₂P Polyhedrons from MOFs Templates with Enhanced Electrochemical Properties for Hydrogen Evolution. *ACS Appl. Mater. Interfaces* **2017**, *9*, 11642–11650. [CrossRef]

82. He, S.; He, S.; Gao, F.; Bo, X.; Wang, Q.; Chen, X.; Duan, J.; Zhao, C. Ni₂P@carbon core-shell nanorod array derived from ZIF-67-Ni: Effect of phosphorization temperature on morphology, structure and hydrogen evolution reaction performance. *Appl. Surf. Sci.* **2018**, *457*, 933–941. [CrossRef]

83. Cai, Z.-X.; Song, X.-H.; Wang, Y.-R.; Chen, X. Electrodeposition-Assisted Synthesis of Ni₂P Nanosheets on 3D Graphene/Ni Foam Electrode and Its Performance for Electrocatalytic Hydrogen Production. *ChemElectroChem* **2015**, *2*, 1665–1671. [CrossRef]

84. Dou, X.; Liu, W.; Liu, Q.; Niu, Z. Nickel Phosphide Nanorod Arrays Vertically Grown on Ni Foam as High-Efficiency Electrocatalyst for the Hydrogen Evolution Reaction. *Chin. J. Chem.* **2017**, *35*, 405–409. [CrossRef]

85. Jung, C.S.; Park, K.; Lee, Y.; Kwak, I.H.; Kwon, I.S.; Kim, J.; Seo, J.; Ahn, J.-P.; Park, J. Nickel phosphide polymorphs with an active (001) surface as excellent catalysts for water splitting. *Crystengcomm* **2019**, *21*, 1143–1149. [CrossRef]

86. Zhou, R.; Zhang, J.; Chen, Z.; Han, X.; Zhong, C.; Hu, W.; Deng, Y. Phase and composition controllable synthesis of nickel phosphide-based nanoparticles via a low-temperature process for efficient electrocatalytic hydrogen evolution. *Electrochim. Acta* **2017**, *258*, 866–875. [CrossRef]

87. Xiao, J.; Lv, Q.; Zhang, Y.; Zhang, Z.; Wang, S. One-step synthesis of nickel phosphide nanowire array supported on nickel foam with enhanced electrocatalytic water splitting performance. *RSC Adv.* **2016**, *6*, 107859–107864. [CrossRef]

88. Tian, T.; Ai, L.; Jiang, J. Metal-organic framework-derived nickel phosphides as efficient electrocatalysts toward sustainable hydrogen generation from water splitting. *RSC Adv.* **2015**, *5*, 10290–10295. [CrossRef]

89. Feng, L.; Vrubel, H.; Bensimon, M.; Hu, X. Easily-prepared dinickel phosphide (Ni₂P) nanoparticles as an efficient and robust electrocatalyst for hydrogen evolution. *Phys. Chem. Chem. Phys.* **2014**, *16*, 5917–5921. [CrossRef]

90. Pu, Z.; Liu, Q.; Tang, C.; Asiri, A.M.; Sun, X. Ni₂P nanoparticle films supported on a Ti plate as an efficient hydrogen evolution cathode. *Nanoscale* **2014**, *6*, 11031–11034. [CrossRef]

91. He, S.; He, S.; Bo, X.; Wang, Q.; Zhan, F.; Wang, Q.; Zhao, C. Porous Ni₂P/C microrods derived from microwave-prepared MOF-74-Ni and its electrocatalysis for hydrogen evolution reaction. *Mater. Lett.* **2018**, *231*, 94–97. [CrossRef]

92. Jeoung, S.; Seo, B.; Hwang, J.M.; Joo, S.H.; Moon, H.R. Direct conversion of coordination compounds into Ni2P nanoparticles entrapped in 3D mesoporous graphene for an efficient hydrogen evolution reaction. *Mater. Chem. Front.* **2017**, *1*, 973–978. [CrossRef]

93. Veeramani, V.; Matsagar, B.M.; Yamauchi, Y.; Badjah, A.Y.; Naushad, M.; Habila, M.; Wabaidur, S.; Alothman, Z.A.; Wang, Z.-L.; Wu, K.C.W. Metal organic framework derived nickel phosphide/graphitic carbon hybrid for electrochemical hydrogen generation reaction. *J. Taiwan Inst. Chem. Eng.* **2019**, *96*, 634–638. [CrossRef]

94. Liu, B.; Wu, C.; Chen, G.; Chen, W.; Peng, L.; Yao, Y.; Wei, Z.; Zhu, H.; Han, T.; Tang, D.; et al. All-in-one surface engineering strategy on nickel phosphide arrays towards a robust electrocatalyst for hydrogen evolution reaction. *J. Power Sources* **2019**, *429*, 46–54. [CrossRef]

95. Wan, L.; Zhang, J.; Chen, Y.; Zhong, C.; Hu, W.; Deng, Y. Varied hydrogen evolution reaction properties of nickel phosphide nanoparticles with different compositions in acidic and alkaline conditions. *J. Mater. Sci.* **2017**, *52*, 804–814. [CrossRef]

96. Zhou, Z.; Wei, L.; Wang, Y.; Karahan, H.E.; Chen, Z.; Lei, Y.; Chen, X.; Zhai, S.; Liao, X.; Chen, Y. Hydrogen evolution reaction activity of nickel phosphide is highly sensitive to electrolyte pH. *J. Mater. Chem. A* **2017**, *5*, 20390–20397. [CrossRef]

97. Ding, Y.; Miao, B.-Q.; Jiang, Y.-C.; Yao, H.-C.; Li, X.-F.; Chen, Y. Polyethylenimine-modified nickel phosphide nanosheets: Interfacial protons boost the hydrogen evolution reaction. *J. Mater. Chem. A* **2019**, *7*, 13770–13776. [CrossRef]

98. Jin, Y.; Zhao, C.; Wang, L.; Jiang, Q.; Ji, C.; He, X. Preparation of mesoporous Ni₂P nanobelts with high performance for electrocatalytic hydrogen evolution and supercapacitor. *Int. J. Hydrog. Energ.* **2018**, *43*, 3697–3704. [CrossRef]

99. Wu, M.-Y.; Da, P.-F.; Zhang, T.; Mao, J.; Liu, H.; Ling, T. Designing Hybrid NiP$_2$/NiO Nanorod Arrays for Efficient Alkaline Hydrogen Evolution. *ACS Appl. Mater. Interfaces* **2018**, *10*, 17896–17902. [CrossRef]

100. You, B.; Jiang, N.; Sheng, M.; Bhushan, M.W.; Sun, Y. Hierarchically Porous Urchin-Like Ni$_2$P Superstructures Supported on Nickel Foam as Efficient Bifunctional Electrocatalysts for Overall Water Splitting. *ACS Catal.* **2016**, *6*, 714–721. [CrossRef]

101. Zhang, T.; Yang, K.; Wang, C.; Li, S.; Zhang, Q.; Chang, X.; Li, J.; Li, S.; Jia, S.; Wang, J.; et al. Nanometric Ni$_5$P$_4$ Clusters Nested on NiCo$_2$O$_4$ for Efficient Hydrogen Production via Alkaline Water Electrolysis. *Adv. Energy Mater.* **2018**, *8*, 1801690. [CrossRef]

102. Liu, T.; Li, A.; Wang, C.; Zhou, W.; Liu, S.; Guo, L. Interfacial Electron Transfer of Ni$_2$P-NiP$_2$ Polymorphs Inducing Enhanced Electrochemical Properties. *Adv. Mater.* **2018**, *30*, 1803590. [CrossRef] [PubMed]

103. Sun, Y.; Zhang, T.; Li, X.; Bai, Y.; Lyu, X.; Liu, G.; Cai, W.; Li, Y. Bifunctional Hybrid Ni/Ni$_2$P Nanoparticles Encapsulated by Graphitic Carbon Supported with N, S Modified 3D Carbon Framework for Highly Efficient Overall Water Splitting. *Adv. Mater. Interfaces* **2018**, *5*, 1800473. [CrossRef]

104. Dinh, K.N.; Sun, X.; Dai, Z.; Zheng, Y.; Zheng, P.; Yang, J.; Xu, J.; Wang, Z.; Yan, Q. O$_2$ plasma and cation tuned nickel phosphide nanosheets for highly efficient overall water splitting. *Nano Energy* **2018**, *54*, 82–90. [CrossRef]

105. Yu, X.; Yu, Z.-Y.; Zhang, X.-L.; Zheng, Y.-R.; Duan, Y.; Gao, Q.; Wu, R.; Sun, B.; Gao, M.-R.; Wang, G.; et al. "Superaerophobic" Nickel Phosphide Nanoarray Catalyst for Efficient Hydrogen Evolution at Ultrahigh Current Densities. *J. Am. Chem. Soc.* **2019**, *141*, 7537–7543. [CrossRef] [PubMed]

106. Yan, L.; Jiang, H.; Xing, Y.; Wang, Y.; Liu, D.; Gu, X.; Dai, P.; Li, L.; Zhao, X. Nickel metal–organic framework implanted on graphene and incubated to be ultrasmall nickel phosphide nanocrystals acts as a highly efficient water splitting electrocatalyst. *J. Mater. Chem. A* **2018**, *6*, 1682–1691. [CrossRef]

107. Ren, J.; Hu, Z.; Chen, C.; Liu, Y.; Yuan, Z. Integrated Ni$_2$P nanosheet arrays on three-dimensional Ni foam for highly efficient water reduction and oxidation. *J. Energy Chem.* **2017**, *26*, 1196–1202. [CrossRef]

108. Yan, Y.; Lin, J.; Bao, K.; Xu, T.; Qi, J.; Cao, J.; Zhong, Z.; Fei, W.; Feng, J. Free-standing porous Ni$_2$P-Ni$_5$P$_4$ heterostructured arrays for efficient electrocatalytic water splitting. *J. Colloid Interface Sci.* **2019**, *552*, 332–336. [CrossRef]

109. Jin, X.; Li, J.; Cui, Y.; Liu, X.; Wang, K.; Zhou, Y.; Yang, W.; Zhang, X.; Zhang, C.; Jiang, X.; et al. In-situ synthesis of porous Ni$_2$P nanosheets for efficient and stable hydrogen evolution reaction. *Int. J. Hydrog. Energ.* **2019**, *44*, 5739–5747. [CrossRef]

110. Lin, Y.; He, L.; Chen, T.; Zhou, D.; Wu, L.; Hou, X.; Zheng, C. Cost-effective and environmentally friendly synthesis of 3D Ni$_2$P from scrap nickel for highly efficient hydrogen evolution in both acidic and alkaline media. *J. Mater. Chem. A* **2018**, *6*, 4088–4094. [CrossRef]

111. Li, J.; Wei, G.; Zhu, Y.; Xi, Y.; Pan, X.; Ji, Y.; Zatovsky, I.V.; Han, W. Hierarchical NiCoP nanocone arrays supported on Ni foam as an efficient and stable bifunctional electrocatalyst for overall water splitting. *J. Mater. Chem. A* **2017**, *5*, 14828–14837. [CrossRef]

112. Li, J.; Yan, M.; Zhou, X.; Huang, Z.-Q.; Xia, Z.; Chang, C.-R.; Ma, Y.; Qu, Y. Mechanistic Insights on Ternary Ni$_{2-x}$Co$_x$P for Hydrogen Evolution and Their Hybrids with Graphene as Highly Efficient and Robust Catalysts for Overall Water Splitting. *Adv. Funct. Mater.* **2016**, *26*, 6785–6796. [CrossRef]

113. Ledendecker, M.; Calderon, S.K.; Papp, C.; Steinrueck, H.-P.; Antonietti, M.; Shalom, M. The Synthesis of Nanostructured Ni$_5$P$_4$ Films and their Use as a Non-Noble Bifunctional Electrocatalyst for Full Water Splitting. *Angew. Chem. Int. Ed.* **2015**, *54*, 12361–12365. [CrossRef] [PubMed]

114. Wang, X.; Kolen'ko, Y.V.; Bao, X.-Q.; Kovnir, K.; Liu, L. One-Step Synthesis of Self-Supported Nickel Phosphide Nanosheet Array Cathodes for Efficient Electrocatalytic Hydrogen Generation. *Angew. Chem. Int. Ed.* **2015**, *54*, 8188–8192. [CrossRef]

115. Mishra, I.K.; Zhou, H.; Sun, J.; Dahal, K.; Ren, Z.; He, R.; Chen, S.; Ren, Z. Highly efficient hydrogen evolution by self-standing nickel phosphide-based hybrid nanosheet arrays electrocatalyst. *Mater. Today Phys.* **2018**, *4*, 1–6. [CrossRef]

116. Cai, W.; Liu, W.; Sun, H.; Li, J.; Yang, L.; Liu, M.; Zhao, S.; Wang, A. Ni$_5$P$_4$-NiP$_2$ nanosheet matrix enhances electron-transfer kinetics for hydrogen recovery in microbial electrolysis cells. *Appl. Energ.* **2018**, *209*, 56–64. [CrossRef]

117. Liu, S.; Hu, C.; Lv, C.; Cai, J.; Duan, M.; Luo, J.; Song, J.; Shi, Y.; Chen, C.; Luo, D.; et al. Facile preparation of large-area self-supported porous nickel phosphide nanosheets for efficient electrocatalytic hydrogen evolution. *Int. J. Hydrog. Energ.* **2019**, *44*, 17974–17984. [CrossRef]

118. Chen, W.; Mishra, I.K.; Qin, Z.; Yu, L.; Zhou, H.; Sun, J.; Zhang, F.; Chen, S.; Wenya, G.E.; Yu, Y.; et al. Nickel phosphide based hydrogen producing catalyst with low overpotential and stability at high current density. *Electrochim. Acta* **2019**, *299*, 756–761. [CrossRef]

119. Wang, X.; Li, W.; Xiong, D.; Petrovykh, D.Y.; Liu, L. Bifunctional Nickel Phosphide Nanocatalysts Supported on Carbon Fiber Paper for Highly Efficient and Stable Overall Water Splitting. *Adv. Funct. Mater.* **2016**, *26*, 4067–4077. [CrossRef]

120. Hu, C.; Cai, J.; Liu, S.; Lv, C.; Luo, J.; Duan, M.; Chen, C.; Shi, Y.; Song, J.; Zhang, Z.; et al. General Strategy for Preparation of Porous Nickel Phosphide Nanosheets on Arbitrary Substrates toward Efficient Hydrogen Generation. *ACS Appl. Energy Mater.* **2019**. [CrossRef]

121. Wu, X.; Guo, Y.; Wang, T.; Sun, B.; Liu, Z.; Wu, Y.; Zhang, S.; Zheng, J.; Li, X. Plasma enabled non-thermal phosphorization for nickel phosphide hydrogen evolution catalysts. *Chem. Commun.* **2019**, *55*, 4202–4205. [CrossRef]

122. Yan, Q.; Chen, X.; Wei, T.; Wang, G.; Zhu, M.; Zhuo, Y.; Cheng, K.; Ye, K.; Zhu, K.; Yan, J.; et al. Hierarchical Edge-Rich Nickel Phosphide Nanosheet Arrays as Efficient Electrocatalysts toward Hydrogen Evolution in Both Alkaline and Acidic Conditions. *ACS Sustain. Chem. Eng.* **2019**, *7*, 7804–7811. [CrossRef]

123. Han, A.; Jin, S.; Chen, H.; Ji, H.; Sun, Z.; Du, P. A robust hydrogen evolution catalyst based on crystalline nickel phosphide nanoflakes on three-dimensional graphene/nickel foam: High performance for electrocatalytic hydrogen production from pH 0–14. *J. Mater. Chem. A* **2015**, *3*, 1941–1946. [CrossRef]

124. Qu, G.; Zhao, Y.; Zhao, G.; Zhou, Y.; Cai, S.; Kang, Y.; Xu, C. Ultrahigh length-to-diameter ratio nickel phosphide nanowires as pH-wide electrocatalyst for efficient hydrogen evolution. *Electrochim. Acta* **2019**, *298*, 943–949. [CrossRef]

125. Bai, Y.; Zhang, H.; Li, X.; Liu, L.; Xu, H.; Qiu, H.; Wang, Y. Novel peapod-like Ni_2P nanoparticles with improved electrochemical properties for hydrogen evolution and lithium storage. *Nanoscale* **2015**, *7*, 1446–1453. [CrossRef]

126. Bai, Y.; Zhang, H.; Fang, L.; Liu, L.; Qiu, H.; Wang, Y. Novel peapod array of Ni_2P@graphitized carbon fiber composites growing on Ti substrate: A superior material for Li-ion batteries and the hydrogen evolution reaction. *J. Mater. Chem. A* **2015**, *3*, 5434–5441. [CrossRef]

127. Miao, M.; Hou, R.; Liang, Z.; Qi, R.; He, T.; Yan, Y.; Qi, K.; Liu, H.; Feng, G.; Xia, B.Y. Chainmail catalyst of ultrathin P-doped carbon shell-encapsulated nickel phosphides on graphene towards robust and efficient hydrogen generation. *J. Mater. Chem. A* **2018**, *6*, 24107–24113. [CrossRef]

128. Lv, X.-W.; Hu, Z.-P.; Chen, L.; Ren, J.-T.; Liu, Y.-P.; Yuan, Z.-Y. Organic–Inorganic Metal Phosphonate-Derived Nitrogen-Doped Core–Shell Ni_2P Nanoparticles Supported on Ni Foam for Efficient Hydrogen Evolution Reaction at All pH Values. *ACS Sustain. Chem. Eng.* **2019**, *7*, 12770–12778. [CrossRef]

129. Wang, M.-Q.; Ye, C.; Liu, H.; Xu, M.; Bao, S.-J. Nanosized Metal Phosphides Embedded in Nitrogen-Doped Porous Carbon Nanofibers for Enhanced Hydrogen Evolution at All pH Values. *Angew. Chem. Int. Ed.* **2018**, *57*, 1963–1967. [CrossRef]

130. Li, G.; Wang, J.; Yu, J.; Liu, H.; Cao, Q.; Du, J.; Zhao, L.; Jia, J.; Liu, H.; Zhou, W. Ni-Ni_3P nanoparticles embedded into N, P-doped carbon on 3D graphene frameworks via in situ phosphatization of saccharomyces with multifunctional electrodes for electrocatalytic hydrogen production and anodic degradation. *Appl. Catal. B: Environ.* **2020**, *261*, 118147. [CrossRef]

131. Cao, X.; Jia, D.; Li, D.; Cui, L.; Liu, J. One-step co-electrodeposition of hierarchical radial Ni_xP nanospheres on Ni foam as highly active flexible electrodes for hydrogen evolution reaction and supercapacitor. *Chem. Eng. J.* **2018**, *348*, 310–318. [CrossRef]

132. Chaudhari, N.K.; Jin, H.; Kim, B.; Lee, K. Nanostructured materials on 3D nickel foam as electrocatalysts for water splitting. *Nanoscale* **2017**, *9*, 12231–12247. [CrossRef]

133. Chen, M.; Qi, J.; Zhang, W.; Cao, R. Electrosynthesis of NiP_x nanospheres for electrocatalytic hydrogen evolution from a neutral aqueous solution. *Chem. Commun.* **2017**, *53*, 5507–5510. [CrossRef]

134. Liu, Q.; Gu, S.; Li, C.M. Electrodeposition of nickel–phosphorus nanoparticles film as a Janus electrocatalyst for electro-splitting of water. *J. Power Sources* **2015**, *299*, 342–346. [CrossRef]

135. Sun, C.; Zeng, J.; Lei, H.; Yang, W.; Zhang, Q. Direct Electrodeposition of Phosphorus-Doped Nickel Superstructures from Choline Chloride–Ethylene Glycol Deep Eutectic Solvent for Enhanced Hydrogen Evolution Catalysis. *ACS Sustain. Chem. Eng.* **2019**, *7*, 1529–1537. [CrossRef]

136. Tang, C.; Asiri, A.M.; Luo, Y.; Sun, X. Electrodeposited Ni-P Alloy Nanoparticle Films for Efficiently Catalyzing Hydrogen- and Oxygen-Evolution Reactions. *ChemNanoMat* **2015**, *1*, 558–561. [CrossRef]

137. Cheng, C.; Shah, S.S.A.; Najam, T.; Zhang, L.; Qi, X.; Wei, Z. Highly active electrocatalysis of hydrogen evolution reaction in alkaline medium by Ni–P alloy: A capacitance-activity relationship. *J. Energy Chem.* **2017**, *26*, 1245–1251. [CrossRef]

138. Wu, R.; Dong, Y.; Jiang, P.; Wang, G.; Chen, Y.; Wu, X. Electrodeposited synthesis of self-supported Ni-P cathode for efficient electrocatalytic hydrogen generation. *Prog. Nat. Sci. Mater. Int.* **2016**, *26*, 303–307. [CrossRef]

139. Ren, Q.; Jin, H.; Xu, X.; Liu, A.; Li, J.; Wang, J.; Wang, S. Hydrogen evolution reaction catalyzed by nickel/nickel phosphide nanospheres synthesized through electrochemical methods. *Electrochim. Acta* **2019**, *298*, 229–236. [CrossRef]

140. Wasalathanthri, R.N.; Jeffrey, S.; Su, N.; Sun, K.; Giolando, D.M. Stoichiometric Control of Electrocatalytic Amorphous Nickel Phosphide to Increase Hydrogen Evolution Reaction Activity and Stability in Acidic Medium. *ChemistrySelect* **2017**, *2*, 8020–8027. [CrossRef]

141. Kim, H.; Park, H.; Kim, D.-K.; Choi, I.; Kim, S.-K. Pulse-electrodeposited nickel phosphide for high-performance proton exchange membrane water electrolysis. *J. Alloy. Compd.* **2019**, *785*, 296–304. [CrossRef]

142. Das, M.; Jena, N.; Purkait, T.; Kamboj, N.; De Sarkar, A.; Dey, R.S. Single-phase Ni_5P_4–copper foam superhydrophilic and aerophobic core–shell nanostructures for efficient hydrogen evolution reaction. *J. Mater. Chem. A* **2019**. [CrossRef]

143. Wang, S.; Zhang, L.; Li, X.; Li, C.; Zhang, R.; Zhang, Y.; Zhu, H. Sponge-like nickel phosphide–carbon nanotube hybrid electrodes for efficient hydrogen evolution over a wide pH range. *Nano Res.* **2017**, *10*, 415–425. [CrossRef]